JCTC Journal of Chemical Theory and Computation

pubs.acs.org/JCTC Article

Modeling of Multiresonant Thermally Activated Delayed Fluorescence Emitters—Properly Accounting for Electron Correlation Is Key!

David Hall, Juan Carlos Sancho-García, Anton Pershin, Gaetano Ricci, David Beljonne, Eli Zysman-Colman,* and Yoann Olivier*

Cite This: J. Chem. Theory Comput. 2022, 18, 4903−4918 Read Online

ACCESS | Metrics & More | Article Recommendations | Supporting Information

ABSTRACT: With the surge of interest in multiresonant thermally activated delayed fluorescent (MR-TADF) materials, it is important that there exist computational methods to accurately model their excited states. Here, building on our previous work, we demonstrate how the spin-component scaling second-order approximate coupled-cluster (SCS-CC2), a wavefunction-based method, is robust at predicting the ΔE_{ST} (i.e., the energy difference between the lowest singlet S_1 and triplet T_1 excited states) of a large number of MR-TADF materials, with a mean average deviation (MAD) of 0.04 eV compared to experimental data. Time-dependent density functional theory calculations with the most common DFT functionals as well as the consideration of the Tamm-Dancoff approximation (TDA) consistently predict a much larger ΔE_{ST} as a result of a poorer account of Coulomb correlation as compared to SCS-CC2. Very interestingly, the use of a metric to assess the importance of higher order excitations in the SCS-CC2 wavefunctions shows that Coulomb correlation effects are substantially larger in the lowest singlet compared to the corresponding triplet and need to be accounted for a balanced description of the relevant electronic excited states. This is further highlighted with coupled cluster singles-only calculations, which predict very different S_1 energies as compared to SCS-CC2 while T_1 energies remain similar, leading to very large ΔE_{ST}, in complete disagreement with the experiments. We compared our SCS-CC2/cc-pVDZ with other wavefunction approaches, namely, CC2/cc-pVDZ and SOS-CC2/cc-pVDZ leading to similar performances. Using SCS-CC2, we investigate the excited-state properties of MR-TADF emitters showcasing large ΔE_{T2T1} for the majority of emitters, while π-electron extension emerges as the best strategy to minimize ΔE_{ST}. We also employed SCS-CC2 to evaluate donor−acceptor systems that contain a MR-TADF moiety acting as the acceptor and show that the broad emission observed for some of these compounds arises from the solvent-promoted stabilization of a higher-lying charge-transfer singlet state (S_2). This work highlights the importance of using wavefunction methods in relation to MR-TADF emitter design and associated photophysics.

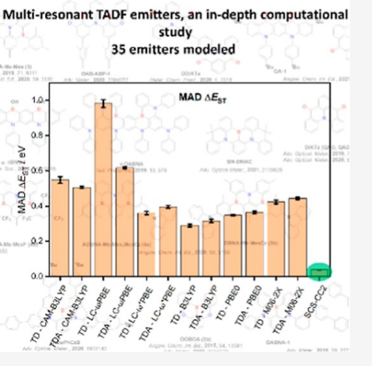

■ INTRODUCTION

Thermally activated delayed fluorescence (TADF) has received significant interest in recent years as materials showing TADF have been demonstrated to act as high-performance emitters in organic light-emitting diodes (OLEDs).[1−4] The mechanism is based on the thermal up-conversion of triplet excitons into singlets via reverse intersystem crossing (RISC). Triplet harvesting in TADF provides a route to 100% internal quantum efficiency (IQE),[5] and a tantalizing alternative family of materials to the state-of-the-art phosphorescent emitters presently used in OLEDs. The design of TADF emitters focuses on the minimization of the energy gap (ΔE_{ST}) between the lowest singlet (S_1) and triplet (T_1) excited states.[6] Although for RISC to occur directly between these two states there must be spin−orbit coupling, and thus the two states must have different orbital types, satisfying El Sayed's rules,[7] ΔE_{ST} remains the primary metric that is optimized in TADF materials development. The most widely used strategy to ensure a small ΔE_{ST} is to couple electron-rich (donor) and electron-poor (acceptor) fragments together covalently (D−A systems) but in a manner where the molecule adopts a highly twisted conformation[5] as this will permit sufficient decoupling of the hole and electron densities associated with the T_1 and S_1 excitations. This produces excited states which are long-range charge transfer (CT) in nature (Figure 1), undergoing distinct solvatochromism.

The huge range of materials showing TADF has been driven in part by the predictive power of the time-dependent density functional theory (TD-DFT) to ably predict ΔE_{ST} at low computational cost. Employing the Tamm−Dancoff approx-

Received: February 10, 2022
Published: July 5, 2022

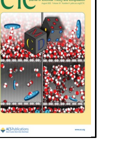

https://doi.org/10.1021/acs.jctc.2c00141
J. Chem. Theory Comput. 2022, 18, 4903−4918

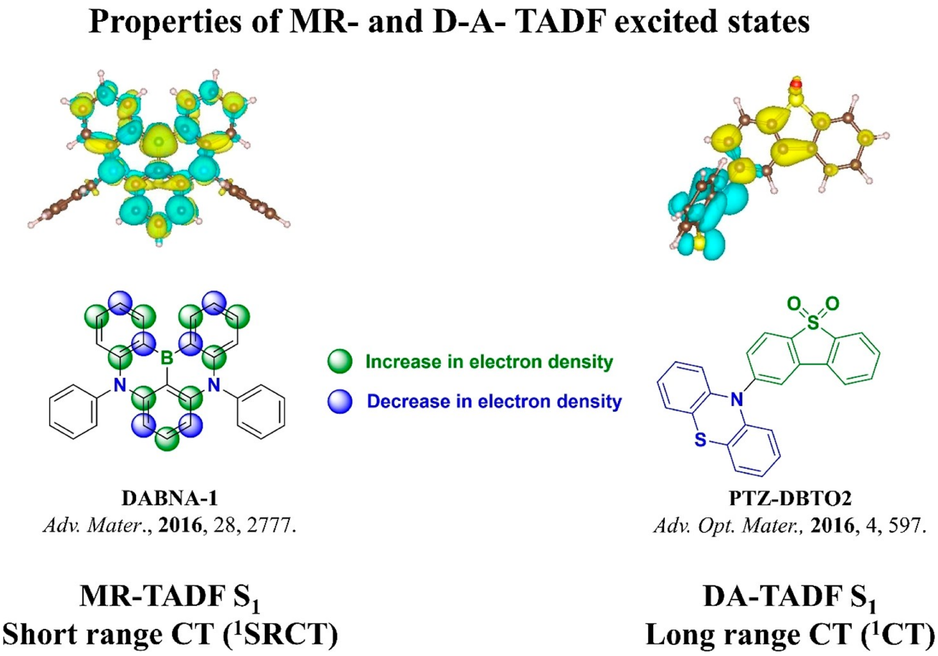

Figure 1. Calculated and simplified difference density plots of the S_1 excited state of prototypical MR-TADF and D−A TADF compounds, (isovalue = 0.001).

imation (TDA-DFT) to TD-DFT provides a more accurate description of the triplet state and thus also ΔE_{ST}, addressing the triplet instability issue present in TD-DFT.[8] Typically, these methods are based on calculations of vertical excitations at the ground-state optimized geometry, which mimic absorption; however, this is often the preferred approach adopted to describe also the excited-state properties of TADF materials, as optimizing excited states is more time consuming.[9] Notably, the diversity of available exchange−correlation functionals often leads to a large range of values for ΔE_{ST}.[10] In the TADF field, several reports exist for D−A systems, showcasing the advantages of some DFT approaches over others.[8,11] Benchmarking DFT functionals against a reference method (often a wavefunction-based method) is necessary in order to make sure a given exchange−correlation can be safely applied to a new class of materials. This way of benchmarking has the advantage of directly comparing similar energy magnitudes in the absence of vibronic and/or solvent effect, which might differ from one experimental study to another, thus making a non-biased comparison difficult.

Within the TADF community calculations center around the use of hybrid functionals such as B3LYP and PBE0, with an exact exchange (xc) contribution of 20[12] and 25%,[13] respectively. Although reports indicate these methods over stabilize CT states,[11] they remain popular as they produce a good agreement between experimentally determined and calculated ΔE_{ST}. However, it must be noted that these agreements essentially arise due to a compensation of errors, and recent work by Champagne and co-workers has suggested that they perform poorly when describing intermediate excited states.[14] Other popular hybrid functionals used include M06-2X, (exact exchange contribution of 54%),[15] which has been shown to improve the correction for the over stabilization of CT states.[14] Range-separated functionals have also been used. In these methods the exchange potential varies depending on whether electron−electron interactions is considered to be long range or short range, with the former being dominated by exact (Hartree−Fock)-exchange and the latter mainly by DFT-like exchange. The range separation parameter ω defines the interelectronic distance (r_{12}) where electron−electron interaction switches from short- to long range. The default value of ω is fixed to 0.400 and 0.330 bohr^{-1} for LC-ωPBE[16] and CAM-B3LYP[17] functionals, respectively. For LC-ωPBE, short-range interactions are described purely using DFT and long-range electron−electron interactions are described only considering exact exchange. In CAM-B3LYP, short- and long-range interactions are described by a combination of both DFT and exact-exchange methods. The value of ω is expected to be material dependent and is often tuned following the protocol proposed by Sun et al.[11] The LC-ω*PBE functional is the ω-tuned version of LC-ωPBE.

Multiresonant TADF (MR-TADF) compounds, an alternative class of TADF materials to D−A compounds, were first introduced by Hatakeyama et al.[18,19] These compounds are designed through the site-specific doping of electron-donating atoms (e.g., nitrogen and oxygen) or withdrawing atoms/functional groups (e.g., boron and ketone groups) of nanographene-like compounds, which leads to a reduction of the exchange interaction and so ΔE_{ST}.[19] In contrast to D−A TADF emitters, the oscillator strength of MR-TADF compounds remains large due to the relatively larger overlap of the HOMO (highest occupied molecular orbital) and LUMO (lowest unoccupied molecular orbital) (Figure 1). MR-TADF materials have a series of distinct properties because of their rigid structures. They show very narrow emission profiles and have small Stokes shifts as there is only minimal reorganization between ground and excited states;[18] they also typically exhibit high photoluminescence quantum yields, Φ_{PL}, due to a synergy between reduced non-radiative decay and increased radiative decay rates, and they show only a minimal positive solvatochromism owing to the short-range CT (SRCT) nature of the excited states.[20]

We recently showed that the poor TD(A)-DFT prediction of ΔE_{ST} can be overcome by relying on wavefunction-based

https://doi.org/10.1021/acs.jctc.2c00141
J. Chem. Theory Comput. 2022, 18, 4903−4918

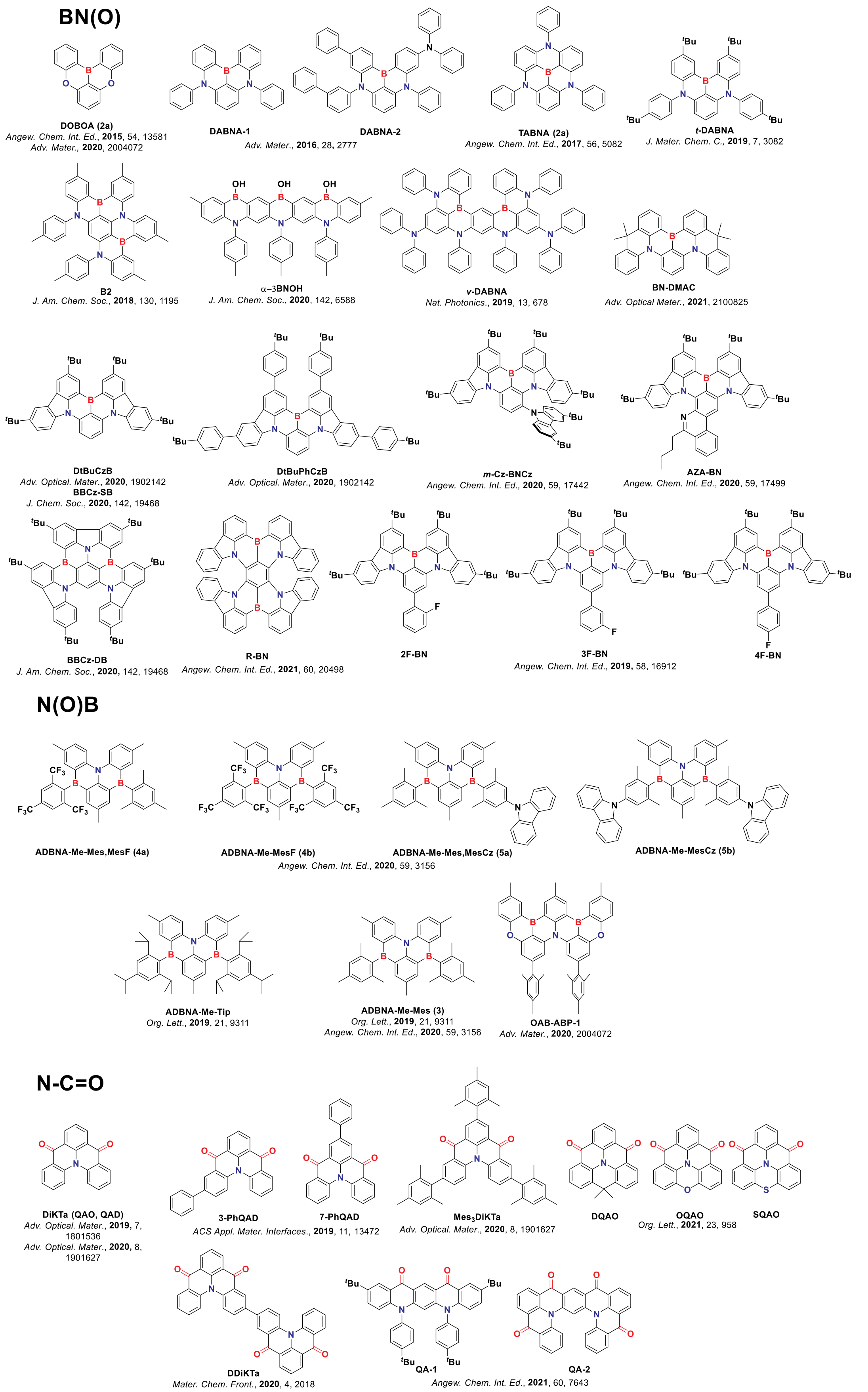

Figure 2. Literature MR-TADF emitters modeled within this study.

https://doi.org/10.1021/acs.jctc.2c00141
J. Chem. Theory Comput. 2022, 18, 4903−4918

methods[21−23] and especially to the spin-component scaling second-order approximate coupled cluster (SCS-CC2) approach.[24] Spin-component scaled (SCS) is a scaling factor introduced for distinguishing between the same spin and opposite spin interactions, resulting in an improved description of correlation effects.[25,26] Coupled cluster calculations can include higher-order excitations (double, triple, etc.) by applying the exponential excitation operator to the Hartree−Fock reference wavefunction. The (perturbative) inclusion of double excitations within SCS-CC2, which are neglected in TD(A)-DFT, is the primary reason for the greater accuracy in predicting ΔE_{ST}, especially in these compounds, where the S_1 state is stabilized thanks to a better description of the Coulomb correlation interaction. However, the increase in accuracy, thanks to the inclusion of higher order electronic excitations, results in an increase in computational cost. The formal scaling of coupled-cluster calculations with single and double excitations (CCSD) is $O(N^6)$, where N reflects the system size in terms of number of basis functions. The computational time can be reduced somewhat to $O(N^5)$ for CC2 as double excitations are partially included.[27] We initially demonstrated that SCS-CC2 calculations provided a good agreement between the experimental and computed ΔE_{ST} for two literature MR-TADF compounds, **DABNA-1** and **TABNA** (**2a**) (Figure 2).[21] We have since used the same methodology to accurately predict the ΔE_{ST} of several other MR-TADF emitters,[20,28−30] and note that SCS-CC2/cc-pVDZ offers a good balance between accuracy and computational cost.[20,28−30] In particular, we were able to compute the accurate values of ΔE_{ST} for the emitters, consisting of more than 100 atoms. Noteworthy, the scaling factor of coupled cluster methods can be reduced even further to N^4 with a spin-opposite scaling (SOS) method,[31] providing a correlated treatment for even larger systems at the costs comparable to TD-DFT. We also acknowledge that second-order algebraic diagrammatic construction [ADC(2)][32] and SCS-ADC(2)[22] that include partially double excitation have also been applied to MR-TADF with some success. However, because these latter methods account for the double excitation in the same vein as SCS-CC2, they were not included in this study.

From a computational point of view, an organic emitter is often assigned to be MR-TADF on the basis of (i) the degree to which the HOMO and LUMO distributions are complementary and (ii) the S_1 oscillator strength, often much larger than D−A systems.[19] However, these parameters do not permit assignment of the SRCT excited state with sufficient accuracy that is the hallmark of MR-TADF emitters, an assignment that is commonly accessible through analysis of the difference density plots (Figure 1). The frequent absence of predicted ΔE_{ST} in the MR-TADF literature is likely an implicit recognition that TD-DFT calculations do not accurately predict this value. From an experimental point of view, in addition to the observed thermally activated delayed fluorescence, MR-TADF behavior is frequently based on (i) the characterization of the full width at half maximum of the emission spectrum, which is expected to be narrow, and (ii) on a small degree of positive solvatochromism. However, these are diagnostic, respectively, only of the rigidity of the compound (i.e., small reorganization of the geometry in the excited state) and of a weakly CT electronic transition. Thus, these criteria should not be used exclusively to infer that the compound is indeed a MR-TADF emitter.

In this work, we have therefore computed the ΔE_{ST}, from the S_1 and T_1 energies of 35 reported MR-TADF emitters at the SCS-CC2/cc-pVDZ level, as well as with TD-DFT and TDA-DFT methods using a wide range of functionals, such as CAM-B3LYP, LC-ωPBE, LC-ω*PBE, B3LYP, PBE0, and M06-2X, all using the 6-31G(d,p) basis set, and the values directly compared to the experiment. We quantify the accuracy of the predictions by assessing the mean average deviation (MAD). Our study reveals that TD-DFT in either its full treatment or within TDA completely fails to accurately predict ΔE_{ST} and that the only way to reach a close agreement with the experiment is through the inclusion of double excitation or higher order excitation that is obtained here using the SCS-CC2 method. Indeed, there is a remarkable MAD of 0.04 eV for predicted ΔE_{ST} across the 35 emitters when SCS-CC2/cc-pVDZ is used, while DFT methods do very poorly, reflected in MAD values roughly ranging between 0.3 and 1.0 eV. The primary reason for the failure of DFT methods lies in the poorly predicted S_1 energies. We investigate other wavefunction approaches such as CC2 and SOS-CC2 and show that these methods, which also include higher order excitations, also perform well. We probed the manifolds of the singlet and triplet excited states of each material with the SCS-CC2 method. We observed that an increase in electronic delocalization leads to a reduction in ΔE_{ST}. Interestingly, ketone-based MR-TADF emitters overall display the largest predicted ΔE_{ST} values. We also observed that very few emitters possess intermediate triplet states between S_1 and T_1. We used the same methodology to investigate the nature of the excited states of 12 compounds that contain a MR-TADF unit acting as an acceptor in a D−A emitter design. In three of these compounds, the CT nature of S_1 is captured. In the nine other compounds, we observed an inversion between the ^{1}CT (S_2) and ^{1}SRCT states in comparison to the experiment. Indeed, the S_2 state is calculated to be relatively close in energy to S_1 and thus given the solid-state polarization or solvent effects, it is not unexpected that the ^{1}CT state is the lowest singlet state observed experimentally.

■ METHODOLOGY

Each of the ground geometries of the 35 MR-TADF emitters was optimized using each of the aforementioned functionals in combination with the 6-31G(d,p)[33] basis set for the DFT methods and the cc-pVDZ[34] basis set for the SCS-CC2 calculations. Note that cc-pVDZ is a basis set of moderate size; however, SCS-CC2 calculations used together with this basis are sufficiently close to those obtained with the larger and more costly def2-TZVP basis set.[24] To further support this observation, we further elaborate on the basis set dependence by performing SCS-CC2 calculations on a limited set of compounds (**DABNA-1**, **DOBNA**, and **DiKTa**, see Figure 2 with their respective chemical structures) with the cc-pVTZ basis set considering their ground-state SCS-CC2/cc-pVTZ geometries (see Section 1e). The DFT functionals used consist of long-range corrected (CAM-B3LYP[17] and LC-ωPBE[16]), optimally tuned LC-ωPBE (LC-ω*PBE[11]), and hybrid functionals (PBE0,[13] B3LYP,[12] and M06-2X[15]). Excited-state energies were calculated using TD-DFT and TDA-DFT (SCS-CC2) from the DFT (SCS-CC2) optimized ground state.[8,11,35] For the SCS-CC2 method, vertical excitations from the ground to the excited states were calculated considering the two first singlet (S_1 and S_2) and the two first triplet excited states (T_1 and T_2). Such calculations are expected to

https://doi.org/10.1021/acs.jctc.2c00141
J. Chem. Theory Comput. 2022, 18, 4903−4918

reasonably model the experimentally measured emission energies owing to the small observed Stokes shifts and limited positive solvatochromism. For further validation of the SCS-CC2 method, CCS, CC2, and SOS-CC2 calculations were carried out on a limited set of compounds (**DABNA-1**, **DOBNA** and **DiKTa**, Figure 2). DFT calculations were performed using Gaussian 16 revision A03[36] while CCS, CC2, SOS-, and SCS-CC2 were performed using Turbomole 7.4.[37]

For each method, we report the MAD, root mean square deviation (RMSD), and standard deviation (σ) for S_1 and T_1 energies as well as ΔE_{ST} over the set of 35 compounds. These are determined according to eqs 1−3, respectively

$$\mathrm{MAD} = \frac{1}{n}\sum_{i=1}^{n} |x_i| \tag{1}$$

$$\mathrm{RMSD} = \sqrt{\frac{1}{n}\sum_{i=1}^{n} \left| x_i \right|^2} \tag{2}$$

$$\sigma = \sqrt{\left(\frac{1}{n}\sum_{i=1}^{n} |x_i|^2\right) - \left(\frac{1}{n}\sum_{i=1}^{n} |x_i|\right)^2} \tag{3}$$

where $x_i = y_i^{\text{Experiment}} - y_i^{\text{Calculated}}$, with $y_i^{\text{Experiment}}$ being either S_1, T_1 energies or ΔE_{ST} obtained from the peak maxima (or the difference thereof) of the fluorescence and phosphorescence spectra in toluene glass at low temperatures (frequently at 77 K). Where possible, we have compared to experimental data obtained under the same experimental conditions to maintain consistency in our analysis. $y_i^{\text{Calculated}}$ refers to the corresponding SCS-CC2, TD(A)-DFT calculations for S_1, T_1, or ΔE_{ST}, and i is the index over the series of $n = 35$ studied molecules. Linear regression analysis was used to assess the predictive power of each method compared to experimental data. A secondary MAD was used to permit cross-comparison between the DFT-calculated oscillator strength and that calculated using SCS-CC2, wherein $x_i = y_i^{\text{SCS-CC2}} - y_i^{\text{DFT}}$.

Difference density plots, Δ, were obtained at the SCS-CC2 level using the following equation

$$\Delta = \rho_{\text{ex}} - \rho_0 \tag{4}$$

where ρ_{ex} is the excited-state density and ρ_0 the ground-state density.

In addition, we computed the electronic difference density Δ_{sing} from the hole and electron densities constructed on the basis of the natural transition orbitals using the Turbomole package. Note that under this approximation, the contribution of double excitations is omitted. As a matter of fact, Δ_{sing} provides a better comparison with TD(A)-DFT and a clearer picture for D−A systems. The attachment and detachment densities were calculated for each DFT functional at both TD-DFT and TDA-DFT levels of theory; these are associated with hole and electron densities. The densities are obtained through a post-analysis of the Gaussian outputs with the NANCY-EX 2.0 software[38,39] They can be related to the difference density using the following equation[40]

$$\Delta = \rho_{\text{A}} - \rho_{\text{D}} \tag{5}$$

where ρ_{A} is the attachment density and ρ_{D} is the detachment density. Comparisons between the nature of S_1 states between SCS-CC2 and DFT were made when comparing Δ with Δ_{sing}. Different density plots were used to visualize the change in electronic density between the ground and excited states and were obtained using the VESTA package.[41] A summary of the emitter structures is in Figure 2, and their photophysical properties are summarized in Table S1.

A design strategy that has been invoked to try and avoid aggregation-caused quenching[20] and/or to enable color tuning[42−45] is to decorate the core MR-TADF structure with either bulky or electron-donor groups, respectively. These groups may affect the nature of the lowest-lying excited states by preferentially stabilizing a CT state over the SRCT state that is localized on the MR-TADF core, resulting in a broadening of the emission and the emergence of a strong positive solvatochromism. To probe this effect, we modeled 12 emitters that contain a MR-TADF core, which may act as an acceptor, and are decorated with pendant electron-donor groups. In each instance the ground state was optimized at the SCS-CC2/cc-pVDZ level of theory, vertical excitation calculations, including S_1, S_2, T_1, and T_2 were performed for each material. The D_{CT}, q_{CT}, and $S_{\pm}$ descriptors were calculated for each emitter in order to distinguish between CT and SRCT states and were calculated from the difference density plots using Multiwfn software package.[46] The first metric, D_{CT}, is the distance between barycenter of the ρ_- (R_-) and ρ_+ (R_+). The larger D_{CT} the greater is the CT character of the transition, with a CT state often quoted as having $D_{\text{CT}} >$ 1.6 Å while an LE state is defined as having a $D_{\text{CT}} <$ 1.6 Å.[47] This metric has some drawbacks for symmetric systems because for strong CT states, the barycenter positions are predicted to be close, leading to small D_{CT} and an unrealistic LE assignment of the nature of the excited state.[47,48] The second metric considered is the charge transferred (q_{CT}), which corresponds to the integrated change in electronic density (either ρ_+ or ρ_-) over the volume on which ρ_+ or ρ_- expand. A value of 1 indicates a CT state and 0 indicates a LE state. The final metric employed is the overlap $S_{\pm}$, which considers the overlap between areas of increased electronic density ρ_+ and decreased electronic density, ρ_-. An overlap $S_{\pm}$ of 1 indicates a LE state, while a value of 0 corresponds to no overlap and thus a CT state. The literature photophysical properties of the emitters are collated in Table S2.

The τ_2 metrics characterizes the contribution of double excitations to the excited-state wavefunctions. It is computed as $\tau_2 = 100\% - \tau_1$, where τ_1 is the contribution from single excitations and defined as

$$\tau_1 = 100 \times \frac{\sum_{ai} E_{ai}^2}{\sum_{ai} E_{ai}^2 + \sum_{i>j}\sum_{a>b} E_{aibj}^2}$$

with E_{ai} and E_{aibj} being the excitations amplitude computed on the singly and doubly excited determinants written in the spin−orbital basis.

■ RESULTS AND DISCUSSION

Benchmarking of MR-TADF Emitters. *ΔE_{ST} Modeling.* Figure 2 shows the chemical structures of the MR-TADF materials selected for this study. The structural diversity of these emitters covers examples across both the full spectral range (λ_{PL} ranging from 390 to 672 nm) but also examples of containing BN(O), N(O)B, and NC═O cores. Photophysical and device data of each of the modeled emitters can be found in Table S1, while the complete calculations set can be found in Tables S3−S37 and Figures S1−S35.

https://doi.org/10.1021/acs.jctc.2c00141
J. Chem. Theory Comput. 2022, 18, 4903−4918

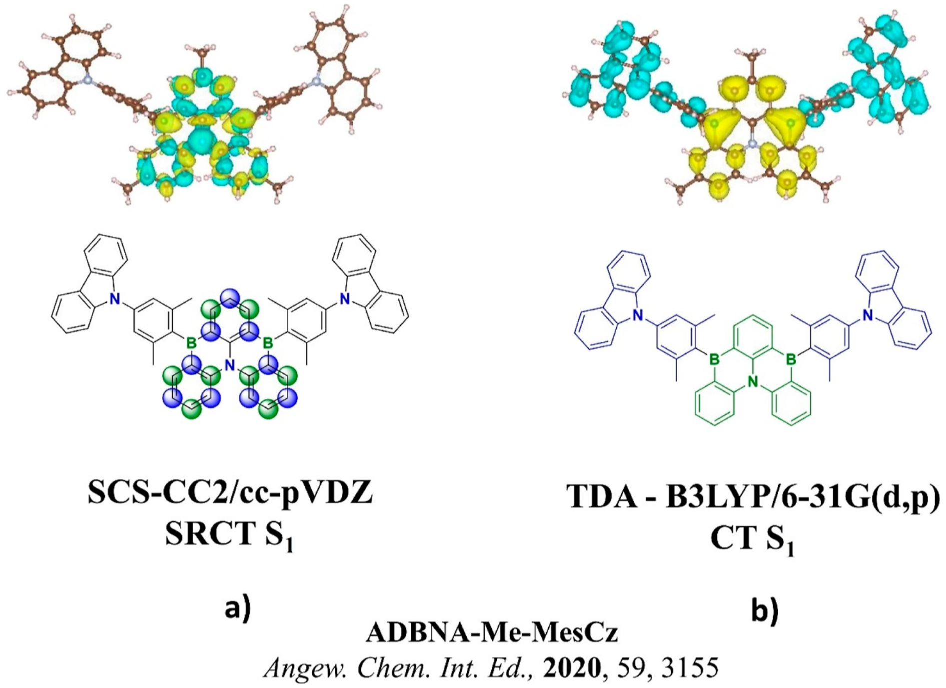

Figure 3. Difference density plots calculated for **ADBNA-Me-MesCz** for the first singlet excited state with (a) SCS-CC2/cc-pVDZ and (b) TDA-B3LYP/6-31G(d,p), where blue balls represent decreased density and green balls increased density, (isovalue = 0.001).

Table 1. MAD and Linear Correlation Coefficient (r^2) of T_1, S_1 and ΔE_{ST} between Computed and Experimental Data

	CAM-B3LYP		LC-ωPBE		LC-ω*PBE		B3LYP		PBE0		M06-2X		
	TD	TDA	TD	TDA	TD	TDA	TD	TDA	TD	TDA	TD	TDA	SCS-CC2
MAD ΔE_{ST}/eV	0.55	0.51	0.98	0.62	0.36	0.40	0.29	0.32	0.35	0.37	0.42	0.44	0.04
r^2 ΔE_{ST}[a]	0.56	0.53	0.04	0.66	0.49	0.39	0.13	0.02	0.56	0.24	0.63	0.37	0.72
MAD S1/eV	0.90	0.99	1.22	1.33	0.47	0.54	0.35	0.41	0.46	0.52	0.86	0.94	0.55
r^2 S_1[a]	0.89	0.94	0.95	0.96	0.88	0.87	0.80	0.73	0.92	0.92	0.90	0.93	0.98
MAD T_1/eV	0.36	0.48	0.33	0.72	0.11	0.15	0.07	0.09	0.11	0.16	0.43	0.49	0.56
r^2 T_1[a]	0.93	0.94	0.60	0.93	0.92	0.91	0.87	0.85	0.93	0.94	0.92	0.92	0.99

[a]Calculated considering only boron emitters.

TD-DFT or TDA-DFT calculations systematically and significantly overestimate ΔE_{ST}. There are, however, two exceptions, **ADBNA-Me-Mes-MesCz** (Table S11 and Figure S9a) and **ADBNA-Me-MesCz** (Tables S13 and S11a), where TDA-B3LYP/6-31G(d,p) and TD-B3LYP/6-31G(d,p) both perform well (the use of the PBE0 functional provides similar results). The experimentally determined ΔE_{ST} for **ADBNA-Me-Mes-MesCz** and **ADBNA-Me-MesCz** are 0.18 and 0.17 eV, respectively, in 1 wt % PMMA,[28] while TDA-B3LYP/6-31G(d,p) and TD-B3LYP/6-31G(d,p) estimated ΔE_{ST} to be, respectively, 0.28 and 0.26 eV for **ADBNA-Me-Mes-MesCz** and 0.18 and 0.21 eV for **ADBNA-Me-MesCz**. ΔE_{ST} was predicted to be 0.17 eV for both compounds using SCS-CC2/cc-pVDZ, which are in excellent agreement with the experimental values. The excited state was assigned experimentally to be SRCT, which is well reproduced by SCS-CC2/cc-pVDZ (Figure 3a) as Δ is localized on adjacent atoms. The SRCT nature was not captured by either TDA-B3LYP/6-31G(d,p) and TD-B3LYP/6-31G(d,p); instead, a ^{1}CT state was predicted (Figures 3b and S56). The observation of an overstabilized CT state has been a well-documented weakness of DFT functionals such as B3LYP and PBE0, and is a consequence of a marked self-interaction error due to their low fraction of exact exchange.[11]

Beyond these two emitters, the DFT calculated ΔE_{ST} was found to be consistently too high regardless of the functional employed; the long-range corrected functionals CAM-B3LYP and LC-ωPBE were the poorest performing (see Table 1 for the MAD values). There is a slight but not significant improvement of the MAD when TDA-DFT calculations are used compared to the TD-DFT calculations, this is due to an improved T_1 description.[8] When the ω value of LC-ωPBE is tuned for each emitter individually, a significant improvement in ΔE_{ST} becomes apparent, with the MAD dropping to 0.36 eV and 0.40 eV for TD-B3LYP/6-31G(d,p) and TDA-B3LYP/6-31G(d,p) calculations, respectively, values that are still much higher than those using SCS-CC2/cc-pVDZ (see Table 1). A gradual decrease in the MAD is observed when hybrid functionals with decreasing exact exchanges are employed, moving from 0.42 eV (0.44 eV) and 0.35 eV (0.37 eV) to 0.29 eV (0.32 eV) for M06-2X, PBE0, and B3LYP using TD-DFT (TDA-DFT), respectively. This observation was previously reported by us, where the LDA functional (with no exact-exchange) performed reasonably well for **DABNA-1** but at the expense of a wrongly predicted nature of the S_1 excited state.[24] When SCS-CC2 is applied, a remarkably small MAD of 0.04 eV is achieved for these compounds, along with a low σ of 0.001 eV. This vastly superior performance is testament to the

https://doi.org/10.1021/acs.jctc.2c00141
J. Chem. Theory Comput. 2022, 18, 4903−4918

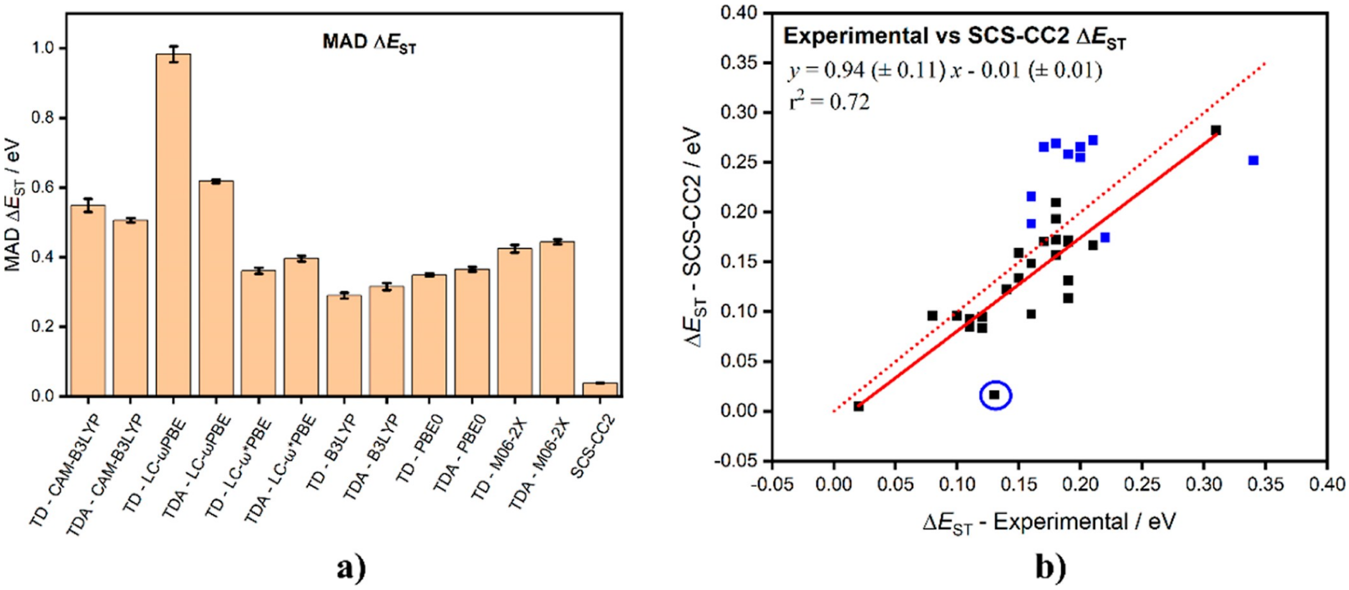

Figure 4. (a) ΔE_{ST} MAD comparing the different computational methodologies with the experiment, and associated error and (b) experimental versus SCS-CC2-calculated vertical ΔE_{ST}, where blue squares denote N−C═O emitters, the red solid line shows the trend line for the data with the N−C═O emitters excluded, and the dotted red line represents the theoretical idealized fit. The blue circle corresponds to **BBCz-DB**, a boron-based emitter.

improved electron correlation description thanks to the (partial) inclusion of double excitations, which is a bottleneck in TD(A)-DFT calculations.

There is only a modest correlation (r^2 of 0.53 for SCS-CC2) between the experimentally determined and calculated ΔE_{ST} (Figure S37a). The r^2 increases to 0.72 when only the boron-containing emitters are included in the analysis (Figure 4). The poorer correlation found when the ketone-containing emitters are included can be understood from the greater degree of positive solvatochromism observed for these molecules compared to the boron-containing compounds (vide infra), which is not captured in our gas-phase calculations. Notably, our prediction for **BBCz-DB** (Figure 4b, blue circle) deviates considerably from the linear fit; it is not clear at this stage what is the origin of this deviation. Compared to SCS-CC2, TD(A)-DFT performs worse, with r^2 ranging between 0.02 and 0.66 when only the boron compounds are included in the data set (Figures S38−S43, Table S39).

Excited-State Energies. In terms of materials development, it is not only important to accurately predict ΔE_{ST} but it is equally essential that the computational methodology accurately predicts the absolute energies of both the S_1 and T_1 states. Owing to the rigid character of MR-TADF compounds, there are small observed Stokes shifts,[18] which supports the use of vertical excitations based on a ground-state optimized geometry as a first approximation to calculating the lowest-lying excited-state energies; the calculated values are thus higher in energy than those experimentally determined. Furthermore, the lack of significantly observed positive solvatochromism in solution,[20] and the minimal impact of polarity in the solid state[49] implies that the inclusion of a solvent continuum model is not required for accurate predictions, thus gas-phase calculations can be used as reasonable predictors for the optoelectronic properties of this class of emitter. For each of the DFT functionals, a large MAD for the S_1 energy was observed. This ranges between 0.90 and 1.33 eV when long-range-corrected functionals CAM-B3LYP and LC-ωPBE at both TD-DFT and TDA-DFT levels are employed, decreasing to 0.47 and 0.54 eV, for TD-DFT and TDA-DFT, respectively, when ω is tuned. When low exact exchange content hybrid functionals are employed, the MAD improves to 0.35 and 0.41 eV for B3LYP at TD-DFT and TDA-DFT, respectively, rising to 0.46 and 0.52 eV for PBE0 at TD-DFT and TDA-DFT, respectively. This increases to 0.86 and 0.94 eV at the TD-DFT and TDA-DFT levels for M06-2X. For SCS-CC2, the MAD for S_1 is 0.55 eV, which is similar to that for the low exact-exchange content functionals (Table 1). There is a remarkable linear correlation (r^2 = 0.98) between experimental and SCS-CC2 calculated S_1 energies, when only the boron-containing emitters are included in the data set (Figure 5a). When the NC═O compounds are also included within the analysis, the r^2 is only 0.69. In these emitters, the influence from solvents and external polarization are more pronounced in line with the stronger positive solvatochromism in comparison to boron-containing compounds.[20,30] In addition, the influence of a difference in the geometrical relaxation between S_1 and T_1 excited states could be a reason for this deviation. For TD(A)-DFT, an improved correlation (r^2 ranging from 0.73 and 0.96) is apparent only when NC═O emitters are omitted; the r^2 ranges values are between 0.61 and 0.84 when all compounds are included in the study (Figures S44−S49 and Tables S40 and S43).

TD(A)-DFT calculations do a much better job of predicting the energy of the T_1 states, reflected in the much smaller MAD values (Figure 5d, Table 1). The smaller MAD observed at TD(A)-DFT for the T_1 in comparison to S_1 highlights the smaller contribution of the Coulomb correlation to the description of the triplet wavefunction. The SCS-CC2 T_1 MAD value is 0.56 eV, which is of the same order as the S_1 MAD (0.55 eV), this is the reason for the remarkably small ΔE_{ST} MAD (Figure 4b). Similarly, to the analysis employed for the comparison of the calculated and experimentally determined S_1 energies, there exists a strongly linear correlation for the T_1 energies (r^2 = 0.99) only when the

https://doi.org/10.1021/acs.jctc.2c00141
J. Chem. Theory Comput. 2022, 18, 4903−4918

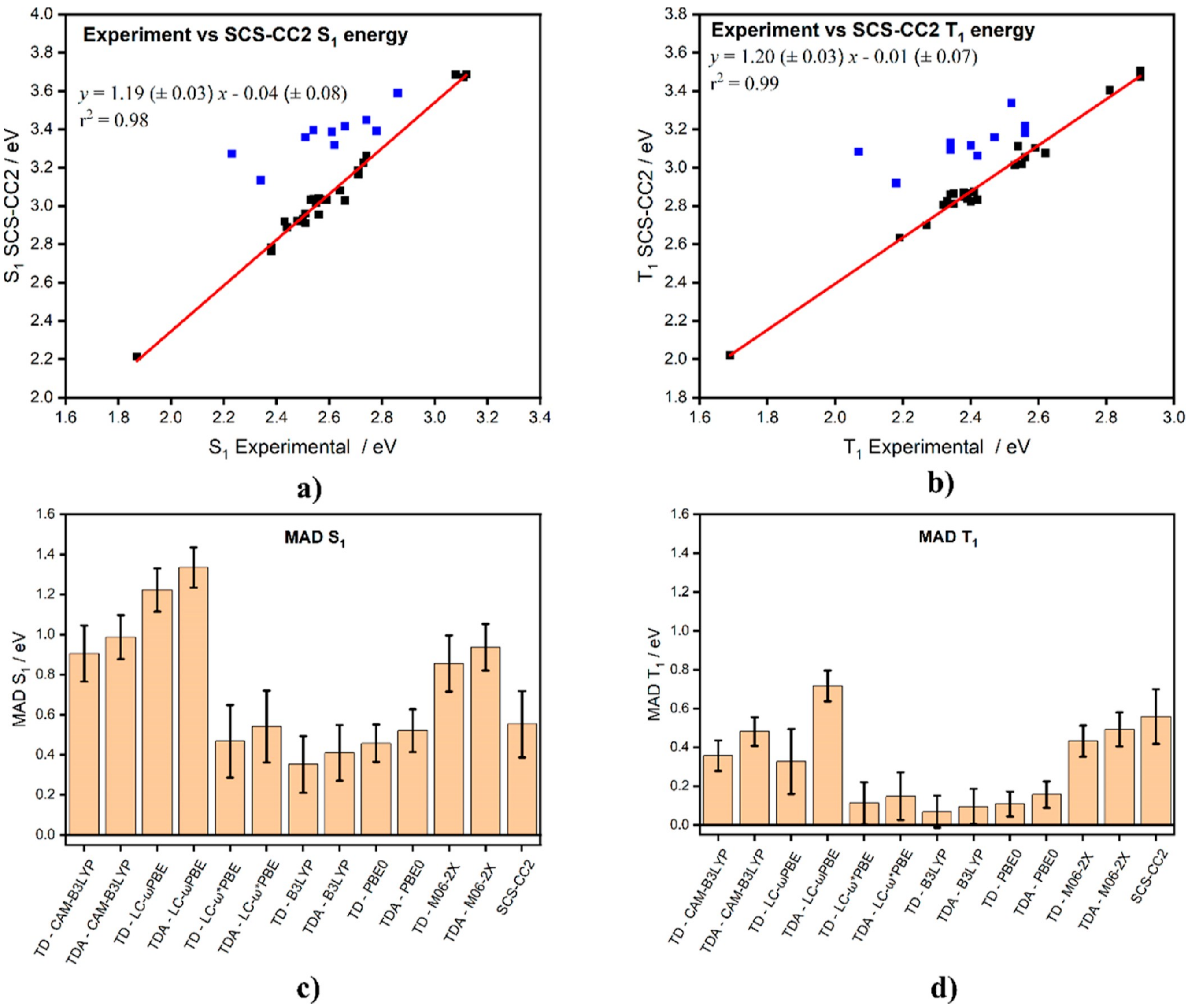

Figure 5. (a) S_1 and (b) T_1 experimental vs SCS-CC2 vertical excitation energies for each emitter. The red lines correspond to a linear fit of the set of data when NC═ are omitted from the fitting and highlighted by blue squares. (c) S_1 and (d) T_1 MAD for both with respect to the experiment.

NC═O emitters are excluded from the data set (Figure 5d). Inclusion of the NC═O emitters results in a poorer correlation (r^2 = 0.71); the calculated T_1 states of the NC═O emitters are higher in energy than those experimentally determined (Figure S37c). DFT functionals perform well, with r^2 values surpassing 0.90 for 9 of the 12 functionals, again this analysis excludes the NC═O emitters (Table S44). Much like that observed for the S_1 analysis, the r^2 values (r^2 ranging from 0.50 to 0.86) decrease when the full data set is considered (Figures S50−S55 and Tables S41).

Oscillator Strength and Excited-State Nature. Taking the SCS-CC2 calculations as the reference method, we evaluated MAD as the difference between the TD(A)-DFT calculated and the SCS-CC2 calculated oscillator strengths (Figure 6a). The MAD values range from 0.04 with TD-CAM-B3LYP to 0.28 with TD-LC-ω*PBE. This analysis seems to suggest that TD(A)-DFT calculations predict a similar S_1 nature as the SCS-CC2 calculations for most compounds. However, upon closer inspection, we observe some significant discrepancies between the difference density patterns predicted between the TD(A)-DFT and SCS-CC2 calculations. For some systems, TD(A)-DFT calculations incorrectly assign S_1 as having either CT or $n-\pi^*$ character, when in fact the S_1 state shows the SRCT character both experimentally and from the SCS-CC2 calculations. For instance, B3LYP and PBE0 both failed to predict the nature of the S_1 state of **ADBNA-Me-MesCz** and **ADBNA-Me-Mes-MesCz** (Figure S56), with a CT excited state predicted. For the ketone-based MR-TADF compounds, TD(A)-DFT/LC-ωPBE, TDA-DFT/LC-ω*PBE, or TD(A)-DFT/M06-2X do not accurately predict the SRCT nature of the S_1 state [**3-PhQAD** (Figure S57), **7-PhQAD** (Figure S58), **Mes$_3$DiKTa** (Figure S59), **DDiKTa** (Figure S60), **QA-2** (Figure S61), **DiKTa** (Figure S62), and **DQAO** (Figure S63)] and instead predict an S_1 state with $n-\pi^*$ character (Figure 7); notably, SCS-CC2 predicts that the S_2 state for these compounds has $n-\pi^*$ character and so it appears that TD(A)-DFT calculations based on these functionals over-stabilize this state at the expense of the SRCT state. Due to the poor predictive ability of most DFT functionals to accurately model the nature of the S_1 state, we would urge researchers to

https://doi.org/10.1021/acs.jctc.2c00141
J. Chem. Theory Comput. 2022, 18, 4903−4918

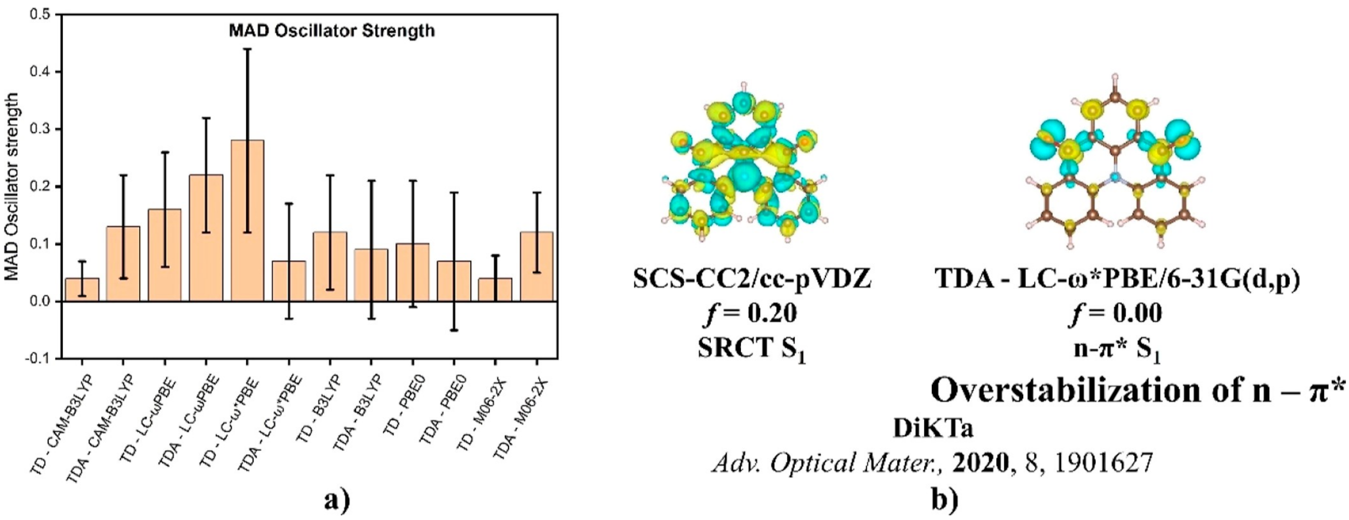

Figure 6. (a) MAD of the oscillator strength between SCS-CC2 and TD(A)-DFT calculations and (b) S_1 excited-state difference density of **DiKTa** for SCS-CC2 and TDA-LC-ω*PBE methods showcasing the difference in the predicted nature of this excited state and their calculated oscillator strength (f) (isovalue = 0.001).

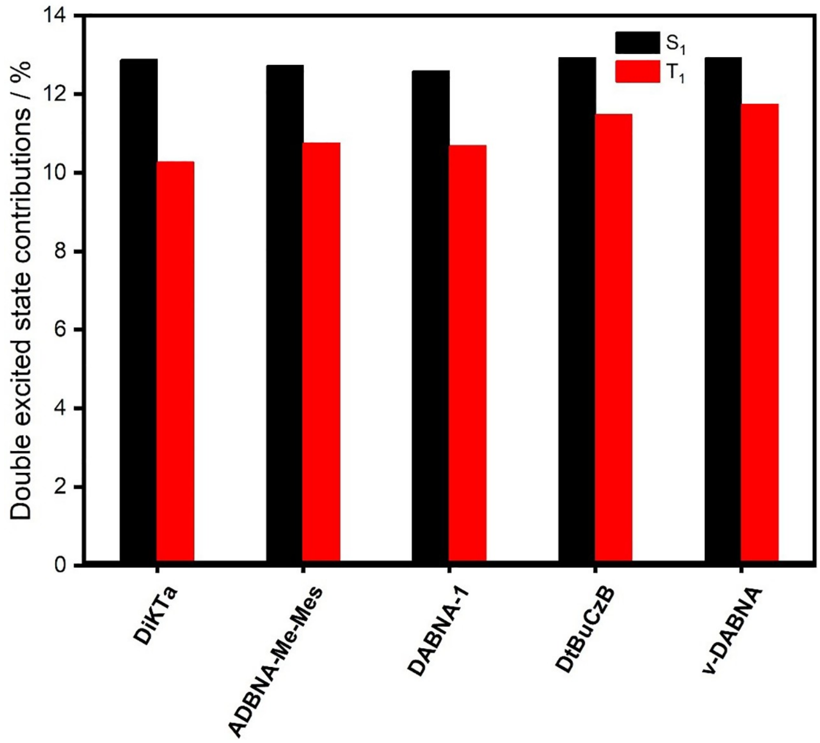

Figure 7. τ_2 values obtained at the SCS-CC2/cc-pVDZ level of theory for five representative molecules out of the set of MR-TADF emitters considered in this study for S_1 (in black) and T_1 (in red) excited states.

not routinely employ these methods for MR-TADF compounds as they may paint an erroneous picture of the excited-state manifold. Of the DFT functionals assessed, owing to its small MAD of 0.04 and small σ of 0.03, we would advocate the use of TD-CAM-B3LYP/6-31G(d,p) to capture S_1 excited-state character if access to SCS-CC2 or other wavefunction-based methods are not available.

Influence of the Basis Set Size and CC2 Spin-Scaling Parameters. In this section, we looked at the influence of the basis set size as well as the spin-scaling of the CC2 method on the energies of the S_1 and T_1 for a set of three materials, **DABNA-1**, **DOBNA** and **DiKTa** which cover the boron-nitrogen-based and ketone-based MR-TADF families. The effect of the spin-scaling of the CC2 method was investigated comparing the spin-component scaled and unscaled CC2 as well as the alternative approach SOS-CC2 considering the cc-pVDZ basis set (see data summarized in Tables S46−S48). For the three compounds investigated, SCS-CC2 shows a slightly smaller deviation from the experimental ΔE_{ST} as compared to CC2 and SOS-CC2 results. More specifically, CC2 slightly overestimates ΔE_{ST} for all compounds in comparison to SCS-CC2 (and the experiments), while SOS-CC2 performs as good as SCS-CC2 for **DABNA-1** and **DOBNA** while largely overestimating ΔE_{ST} for **DiKTa**. We also looked at the basis

https://doi.org/10.1021/acs.jctc.2c00141
J. Chem. Theory Comput. 2022, 18, 4903−4918

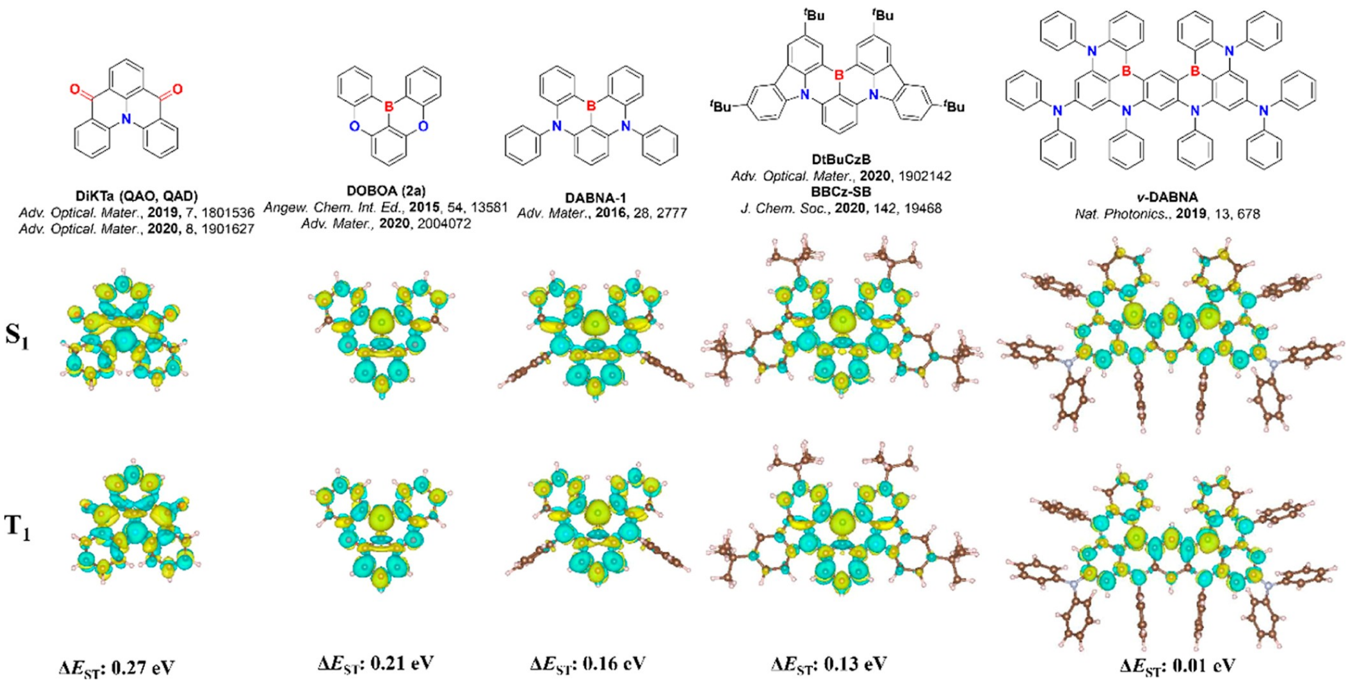

Figure 8. Difference density patterns and ΔE_{ST} obtained at the SCS-CC2/cc-pVDZ level of theory for calculated emitters (isovalue = 0.001).

set effect comparing SCS-CC2 excited-state energies and ΔE_{ST} obtained with the cc-pVDZ and cc-pVTZ basis sets. Overall, the energies of the S_1 and T_1 are hardly affected resulting in an identical ΔE_{ST} prediction with the two basis sets for **DOBNA** and **DABNA-1**, while a slight improvement (0.02 eV) was apparent for **DiKTa**; however, at a prohibitive computational cost.

Double Excitation Contribution to the Excited-State Wavefunctions. We next computed the τ_2 metric, which measures the contribution from double excitations to the excited-state wavefunction.[50] In Figure 7, we report the τ_2 values for five representative molecules (**DABNA-1**, **DiKTa**, **BCz-BN**, **ADBNA-Me-Mes**, and *ν*-DABNA, the results for all molecules are presented in Figure S64) out of the set of MR-TADF emitters considered, covering a range of ΔE_{ST} from 0.01 to 0.27 eV. Interestingly, we find that double excitations contribute significantly to the wavefunctions of the lowest singlet and triplet excited states and that τ_2 is systematically larger in S_1 with respect to T_1 leading to a larger contribution of the Coulomb correlation in the singlet compared to the triplet that reduces the singlet−triplet gap and brings it to values closer to the experiment. CCS/cc-pVDZ calculations (which do not include double excitations) predict a large deviation of S_1 energies with respect to SCS-CC2/cc-pVDZ for a test set of three emitters (**DABNA-1**, **DOBNA**, and **DiKTa**), while T_1 energies remain similar with both methods. Consequently, each compound displays a CCS ΔE_{ST} much larger (>1.36 eV) than the experimental (<0.18 eV) and the SCS-CC2 (<0.27 eV) ones highlighting again the essential role played by double excitations to account properly for the electron correlation contribution for the accurate calculation of the S_1 energies and hence ΔE_{ST}

Discussion on the RISC Mechanism of MR-TADF Emitters from an SCS-CC2 Perspective. Our calculations with the SCS-CC2 method revealed that NC═O emitters have a larger predicted ΔE_{ST}, ranging between 0.17 and 0.27 eV, while the boron-containing compounds (excluding ***α*-3BNOH**) have ΔE_{ST} ranging between 0.01 and 0.21 eV. When comparing **DiKTa** (ΔE_{ST} = 0.27 eV), **DABNA-1** (ΔE_{ST} = 0.16 eV), and **DOBNA** (ΔE_{ST} = 0.21 eV), **DiKTa** has the larger ΔE_{ST} (Figure 8). When analyzing q_{CT} and D_{CT}, we observed that **DABNA-1** (**DiKTa**) S_1 and T_1 excited states exhibit the largest (lowest) CT character and thus, the lowest (largest) ΔE_{ST} (see Table 2).

Table 2. CT Metrics for DABNA-1, DOBNA, and DiKTa Calculated with SCS-CC2/cc-pVDZ

		T_1		ΔE_{ST}/eV	
compound	S_1	D_{CT}/Å	q_{CT}	D_{CT}/Å	q_{CT}
DiKTa	0.81	0.59	0.61	0.59	0.27
DOBNA	0.84	0.57	0.68	0.61	0.20
DABNA-1	0.89	0.63	0.75	0.67	0.16

The largest ΔE_{ST} of the 35 compounds is observed for ***α*-3BNOH**, at 0.28 eV, while the smallest calculated ΔE_{ST} are for *ν*-DABNA (0.01 eV) and **BBCz-DB** (0.02 eV). For *ν*-DABNA, this is likely due to the increased electronic delocalization of the S_1 and T_1 excited-state difference density (Figure 8) minimizing the exchange interaction energy. We are uncertain as to the origin of the low ΔE_{ST} in **BBCz-DB** but note the unusually poor prediction compared to experimental ΔE_{ST} (Figure 4, blue circle). **OAB-ABP-1** shows a smaller ΔE_{ST} of 0.08 eV compared to other nitrogen-centered emitters, likely linked to the extended π delocalization afforded by the bridging oxygen atoms. This π-delocalization is the primary means to reduce ΔE_{ST} and explains the modest decrease in ΔE_{ST} when carbazole moieties are incorporated into the molecule as in **2F-BN**, **3F-BN**, **4F-BN**, **DtBuCzBN**, **DtBuPhCzBN**, **m-CzBNCz**, and **AZA-BN** compared to **DABNA-1** (ΔE_{ST} 0.08−0.13 eV compared to 0.16 eV).

A similar character for the S_1 and T_1 states is observed for each of these emitters, based on an analysis of their difference density patterns (Figures S65−S72), which would suggest

https://doi.org/10.1021/acs.jctc.2c00141
J. Chem. Theory Comput. 2022, 18, 4903−4918

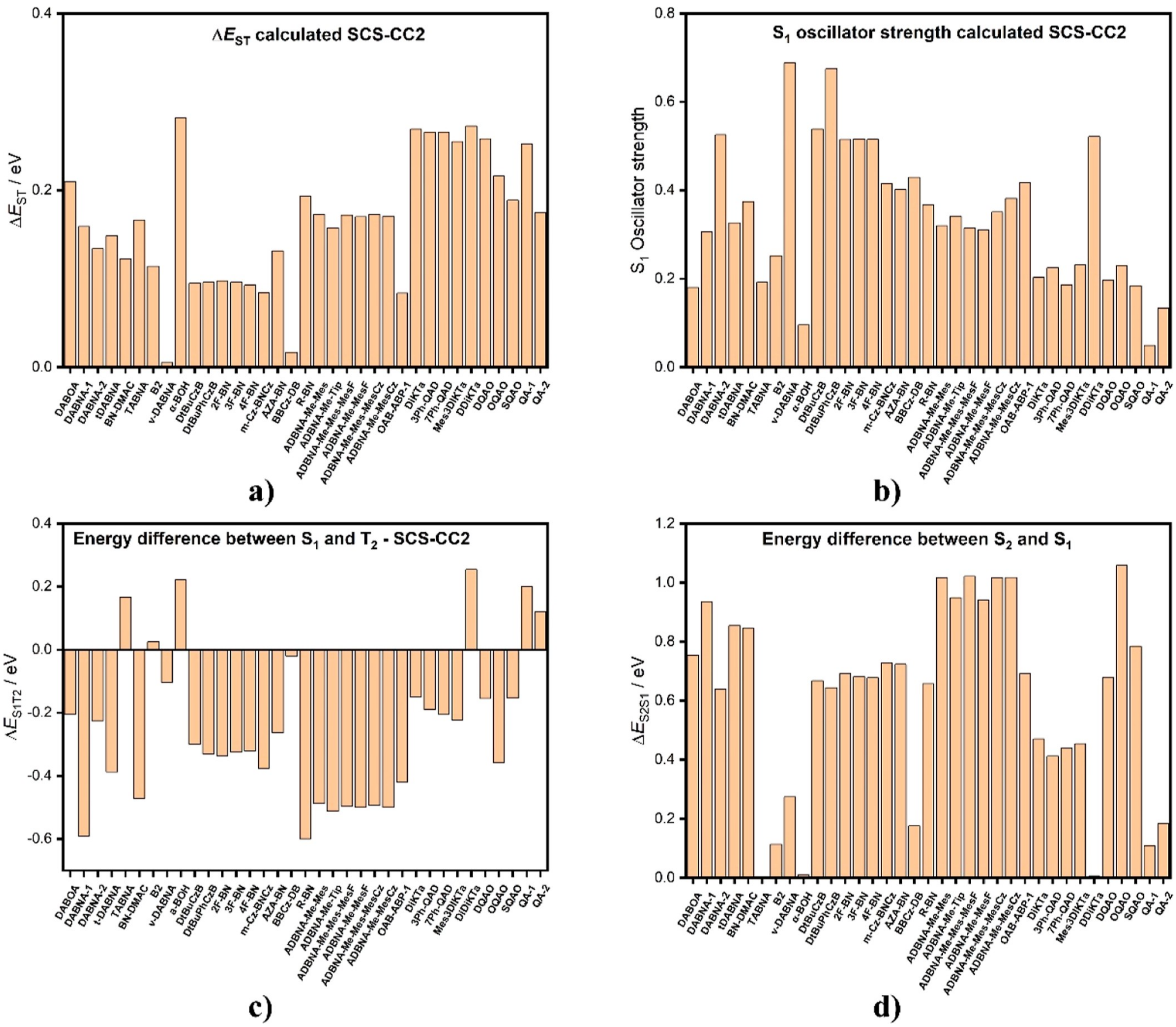

Figure 9. Changing properties of each of the MR-TADF emitters calculated at SCS-CC2/cc-pVDZ, where (a) ΔE_{ST}, (b) S_1 oscillator strength, (c) energy difference between S_1 and T_2, and (d) energy difference between S_2 and S_1.

small spin-orbit coupling between these two states.[7] Potentially, a higher lying triplet and singlet states could be involved in mediating RISC.[7,51−53] In MR-TADF, RISC has been postulated to take place either via a super exchange mechanism[54] or similarly as with D−A TADF materials via a spin-vibronic mechanism. For most of the compounds, in this study, T_2 is calculated to be much higher in energy than S_1 (Figure 9c), thus suggesting that its involvement in RISC is minimal. There are, however, several exceptions, namely, **α-3BNOH**, **DDiKTa**, **B2**, **QA-1**, *ν*-DABNA, and **QA-2**. Notably, **DDiKTa**, *ν*-DABNA, and **QA-2**, which all show very efficient RISC rates,[29,30,55] consistent with the involvement of T_2 facilitating RISC. Generally, smaller ΔE_{S1T2} is observed for the NC═O emitters (Figure 9), which may explain the observed k_{RISC} values despite their larger calculated ΔE_{ST}. The position of higher lying singlet states has also been conjectured to facilitate RISC in MR-TADF emitters;[56] however, in the majority of examples, S_2 is calculated to be more than 0.4 eV destabilized compared to S_1 (Figure 9d), rendering its influence to the RISC mechanism to be minimal. Several exceptions exist where each of **α-3BNOH**, **DDiKTa**, **B2**, **QA-1**, and **QA-2** have low-lying S_2 states. We also note that *ν*-DABNA and **BBCz-DB** possess smaller calculated S_1−S_2 gaps. A similar nature of S_1 and T_1, and the large ΔE_{S1T2} and ΔE_{S2S1} may explain why MR-TADF emitters exhibit much slower k_{RISC} values than the highest performing D−A systems.

Modeling of Emitters that Contain MR-TADF Core Structures but That Are not MR-TADF. An increasingly popular TADF molecular design is to use MR-TADF core structures as rigid acceptor units in formally D−A TADF systems.[28,57−64] When a donor is sufficiently strong, the CT state becomes the lowest lying state while the characteristic SRCT state of MR-TADF emitters is relegated to a higher lying excited state. The result of this design is a compound with an emission that is much broader and is more responsive to the polarity of the medium (Figure 1) than conventional MR-TADF emitters.

https://doi.org/10.1021/acs.jctc.2c00141
J. Chem. Theory Comput. 2022, 18, 4903−4918

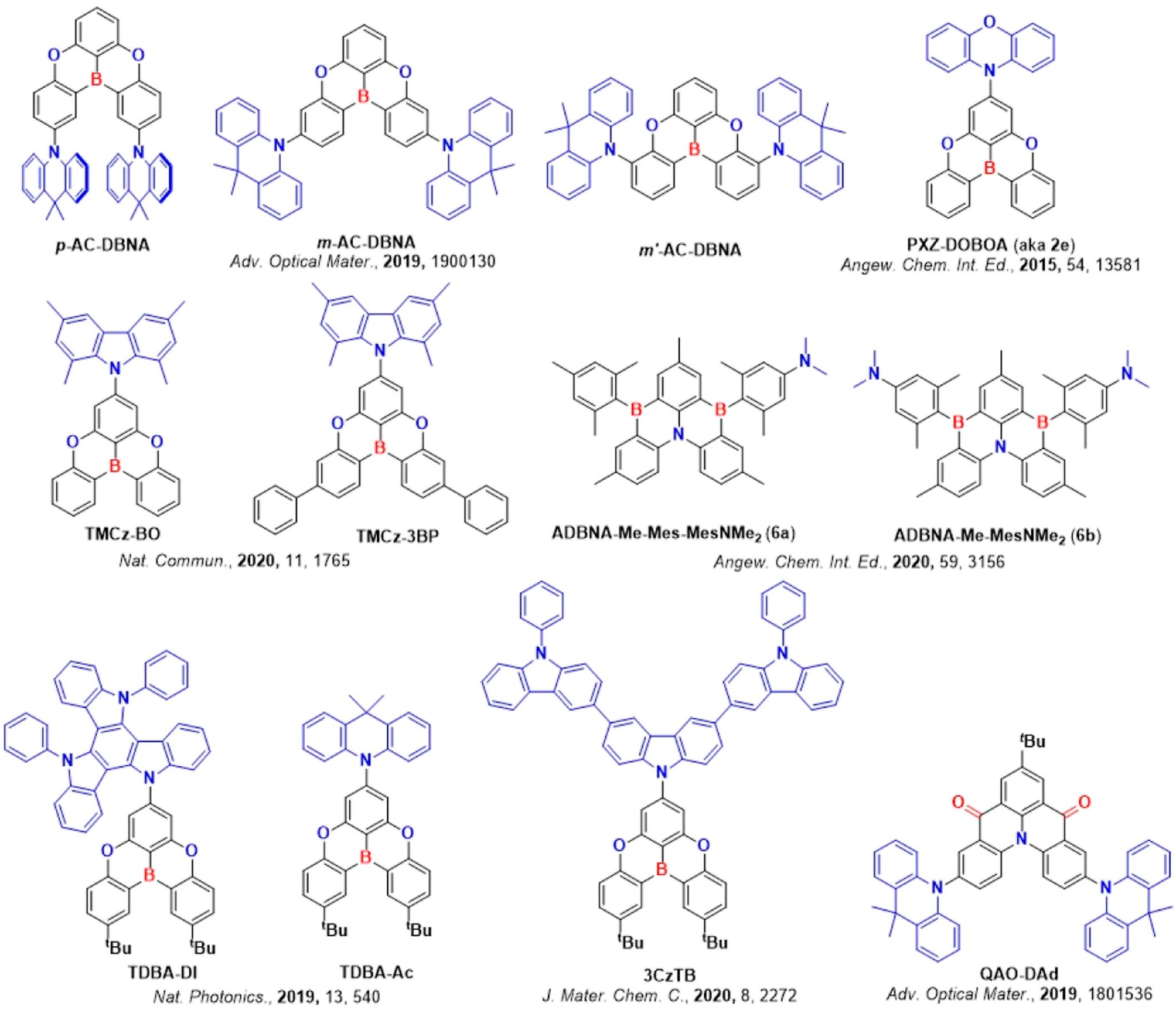

Figure 10. Structures of modeled D−A TADF emitters, which have a MR-TADF unit.

Table 3. Calculated Excited-State Natures of S_1 and S_2 for DOBNA, PXZ-DOBNA, *m*-AC-DBNA, and *p*-AC-DBNA

	S_1					S_2				
compound	energy/eV	D_{CT}/Å	q_{CT}	$S_\pm$	excited state	energy/eV	D_{CT}/Å	q_{CT}	$S_\pm$	excited state
DOBNA	3.68	1.57	0.58	0.92	SRCT	N/A	N/A	N/A	N/A	N/A
PXZ-DOBNA	3.38	5.30	0.95	0.23	CT	3.67	1.31	0.58	0.94	SRCT
p-**AC-DBNA**	3.51	1.96	0.94	0.51	CT	3.52	1.95	0.94	0.51	CT
***m*-AC-DBNA**	3.47	3.68	0.79	0.62	CT	3.52	4.34	0.91	0.32	CT

Recognizing the importance to accurately model the excited-state manifold of this subclass of D−A systems, we performed SCS-CC2 calculations focusing on the nature of both the S_1 and S_2 states of 12 emitters, each of which contains a MR-TADF acceptor moiety but where experimentally, the compound shows a broad emission spectrum and significant positive solvatochromism (Figure 10). A full summary of the photophysical and device data can be found in Table S2. In each case, the degree of CT character was determined, which acts as a metric for assigning the state as either SRCT or CT (Tables 3sifile1 and 4 and Table S49), along with the difference density plots (Figures S73−S77); the difference density plots of the MR-TADF moieties **DiKTa**, **DOBNA**, and **ADBNA-Me-Mes** are shown in Figure S73. When employing a ground-state optimized geometry, SCS-CC2 incorrectly predicts a S_1 state with the SCRT character for most of these compounds; only for **PXZ-DOBNA**, ***m*-AC-DBNA**, and ***p*-AC-DBNA** do the SCS-CC2 calculations accurately predict the CT character of the S_1 state (Figure S74, Table 3). Each of these three latter compounds contains the same common MR-TADF acceptor moiety based on **DOBNA**.

For nine of the emitters (***m′*-AC-DBNA**, **QAO-DAd**, **TBNA-Ac**, **TBNA-DI**, **ADBNA-Me-MesNMe2**, **ADBNA-Me-Mes-MesNMe2**, **TMCz-BO**, **TMCz-3BP**, and **3CzTB**),

https://doi.org/10.1021/acs.jctc.2c00141
J. Chem. Theory Comput. 2022, 18, 4903−4918

Table 4. Calculated Excited State S_1 and S_2 Energies and Their Associated CT Descriptors for D−A Emitters Incorporating a MR-TADF Core as an Acceptor as Well as the MR-TADF Core Alone

	S_1					S_2				
compound	energy/eV	D_{CT}/Å	q_{CT}	$S_\pm$	excited state	energy/eV	D_{CT}/Å	q_{CT}	$S_\pm$	excited state
DOBNA	3.68	1.57	0.58	0.92	SRCT	N/A	N/A	N/A	N/A	N/A
ADBNA-Me-Mes	3.04	1.34	0.63	0.94	SRCT	N/A	N/A	N/A	N/A	N/A
DiKTa	3.45	1.45	0.59	0.91	SRCT	N/A	N/A	N/A	N/A	N/A
***m′*-AC-DBNA**	3.56	1.84	0.61	0.89	SRCT	3.69	1.76	0.95	0.62	CT
QAO-DAd	3.37	1.17	0.59	0.93	SRCT	3.45	5.12	0.91	0.33	CT
TBNA-Ac	3.57	1.14	0.59	0.95	SRCT	3.61	5.28	0.95	0.24	CT
TBNA-DI	3.56	1.45	0.59	0.93	SRCT	3.69	5.12	0.62	0.62	CT
ADBNA-Me-MesNMe2 (6b)	3.05	1.29	0.63	0.94	SRCT	3.57	1.73	0.91	0.67	CT
ADBNA-Me-Mes-MesNMe2 (6a)	3.04	1.31	0.63	0.94	SRCT	3.56	4.97	0.92	0.37	CT
TMCz-BO	3.65	1.37	0.58	0.95	SRCT	3.81	5.51	0.95	0.34	CT
TMCz-3BP	3.58	1.42	0.59	0.94	SRCT	3.74	5.8	0.93	0.24	CT
3CzTB	3.61	1.01	0.58	0.97	SRCT	3.78	5.70	0.74	0.47	CT

SCS-CC2 calculations predict a SRCT S_1 state, while a close-lying S_2 state displays pronounced CT character (Table 4 and Figures S75−S77); the SRCT nature of the S_1 state is based on similar D_{CT}, q_{CT}, and $S_\pm$ values of these compounds compared to those of the MR-TADF acceptor moiety only. When analyzing the nature of the S_2 state of these compounds, we observed both D_{CT} and q_{CT} increasing with respect to S_1 while $S_\pm$ decreased. Among the different compounds, ***m′*-AC-DBNA** has a smaller D_{CT} (S_1 1.84 Å, S_2 1.76 Å), but this is readily explained by the symmetry of this compound, which usually biases the D_{CT}. However, based on q_{CT} and $S_\pm$, we confirm the long-range CT character of the S_2 state.[65] Each material had a difference density pattern for the S_2 state that is reminiscent of a long-range CT state. **ADBNA-Me-MesNMe2** and **ADBNA-Me-Mes-MesNMe2** have the same electron-accepting MR-TADF moiety. **ADBNA-Me-Mes** has D_{CT} of 1.34 Å, q_{CT} of 0.63, and $S_\pm$ of 0.94, values all similar to those calculated for other MR-TADF emitters. The S_1 state of **ADBNA-Me-MesNMe2** and **ADBNA-Me-Mes-MesNMe2** are assigned as SRCT, while S_2 has the long-range CT character. Finally, **QAO-DAd**, which contains a **DiKTa** accepting moiety, has D_{CT}, q_{CT}, and $S_\pm$ values all consistent with an S_1 state of SRCT character, while S_2 is of long-range CT character.

Another element that could drive the S_1−S_2 state inversion is the potential difference in geometry relaxation energy in the excited state that could exist between SRCT and long-range CT states and which is neglected in vertical excitation calculations. Thus, in polar media, a broad CT emission could be observed, whereas the gas-phase calculations predict a S_1 state with a SRCT (Figure S74). Owing to their large S_1−S_2 energy gap (0.52 eV), both **ADBNA-Me-MesNMe$_2$** and **ADBNA-Me-Mes-Mes-NMe$_2$** display experimentally two clear distinct bands in the solvatochromic screen[28] as exemplified by the emission spectrum of **ADBNA-Me-Mes-MesNMe$_2$** in CH_2Cl_2 where dual emission is observed. We assign the high energy band to emit from the SRCT state as it is of similar energy to other structurally similar MR-TADF emitters in the study, and the second low energy band to the CT emission. This example illustrates the importance of modeling both the S_1 and S_2 states of this class of compound.

■ CONCLUSIONS

Using TD(A)-DFT and SCS-CC2 calculations, we have investigated MR-TADF emitters and materials bearing a MR-TADF core as acceptors in an effort to establish an accurate methodology to predict both ΔE_{ST} and the nature of the low-lying excited states of these compounds. Reaffirming our previous works, we demonstrate the robustness of the ΔE_{ST} prediction when applying the SCS-CC2 method in comparison to TD(A)-DFT, as evidenced by an extremely small MAD value of 0.04 eV reported across 35 MR-TADF emitters. The overestimation observed at the TD(A)-DFT level is consistent for the set of functionals investigated and we assigned it to the poorly predicted S_1 energy due to an inaccurate account of Coulomb electron correlations. We would encourage the community with an interest in the design of MR-TADF materials to ensure they employ a computational methodology that includes (at least partially) double excitation as supported by the comparison between CCS and SCS-CC2 calculations. The use of such a methodology not only improved excited-state energy prediction but also the description of the short-range CT nature of the lower lying singlet and triplet excited states, a unique feature of this class of emitters. These conclusions obtained with the SCS-CC2/cc-pVDZ are largely confirmed by (i) methods characterized by a different parameterization of the opposite and same spin electron−electron interactions such as CC2 and SOS-CC2 and (ii) a larger cc-pVTZ basis set. With SCS-CC2, our method of choice, we observed a decrease in ΔE_{ST} when electron delocalization is increased, and when boron is used in place of ketone. We also characterized the higher lying S_2 and T_2 excited states, which appear to be in most cases much higher in energy compared to the lower lying singlet and triplet excited states. Unlike conventional D−A TADF materials, there is only a small fraction of MR-TADF materials that displays energetically closely lying triplet states, whose involvement is believed to facilitate RISC. The slow k_{RISC} measured experimentally for most of the compounds are supported by the very large T_1−T_2, S_1−T_2, and S_1−S_2 energy gaps, suggesting that a spin-vibronic mechanism as observed in D−A TADF is inefficient in MR-TADF compounds. This potentially supports alternative routes for MR-TADF triplet harvesting, which have recently been proposed via the host−guest exciplex state.[66] Owing to the computational cost of wavefunction-based approaches, we anticipate that the community might be reluctant to adopt such an approach, often preferring TD(A)-DFT. TD(A)-DFT not only fails in predicting the excited-state energies but it also fails in disclosing the nature of S_1 for most of the functionals with the exception of CAM-B3LYP. In compounds containing a

https://doi.org/10.1021/acs.jctc.2c00141
J. Chem. Theory Comput. 2022, 18, 4903−4918

MR-TADF core that acts as an acceptor in D–A TADF emitters, we demonstrated that gas-phase SCS-CC2 calculations predicts S_1 and S_2 to be always of SRCT and long-range CT characters, respectively. Because of the strong dependence of the emission properties as a function of the polarity of the solvent in these compounds, it is possible that there is a switch from the narrow SRCT-like to a broad CT-like emission as observed in ref.[28] We therefore conclude that a proper account of solvent effects as implemented recently in antiadiabatic approaches that go beyond commonly used (adiabatic) continuum models,[67] or quantum mechanics/molecular mechanics simulations[68] together with excited-state geometry relaxation are required in order to account for the potential S_1–S_2 state inversion between the SCRT and the long-range CT excited states in this class of compounds.

■ ASSOCIATED CONTENT

Supporting Information

The Supporting Information is available free of charge at https://pubs.acs.org/doi/10.1021/acs.jctc.2c00141.

Photophysical and device data of studied emitters and computational data of all studied emitters along with coordinates (PDF)

■ AUTHOR INFORMATION

Corresponding Authors

Eli Zysman-Colman – *Organic Semiconductor Centre, EaStCHEM School of Chemistry, University of St Andrews, KY16 9ST St Andrews, U.K.*; orcid.org/0000-0001-7183-6022; Email: eli.zysman-colman@st-andrews.ac.uk; http://www.zysman-colman.com

Yoann Olivier – *Laboratory for Computational Modeling of Functional Materials, Namur Institute of Structured Matter, Université de Namur, 5000 Namur, Belgium*; orcid.org/0000-0003-2193-1536; Email: Yoann.Olivier@umons.ac.be

Authors

David Hall – *Organic Semiconductor Centre, EaStCHEM School of Chemistry, University of St Andrews, KY16 9ST St Andrews, U.K.; Laboratory for Chemistry of Novel Materials, University of Mons, 7000 Mons, Belgium*

Juan Carlos Sancho-García – *Department of Physical Chemistry, University of Alicante, E-03080 Alicante, Spain*; orcid.org/0000-0003-3867-1697

Anton Pershin – *Wigner Research Centre for Physics, Budapest 1121, Hungary*; orcid.org/0000-0002-2414-6405

Gaetano Ricci – *Laboratory for Computational Modeling of Functional Materials, Namur Institute of Structured Matter, Université de Namur, 5000 Namur, Belgium*

David Beljonne – *Laboratory for Chemistry of Novel Materials, University of Mons, 7000 Mons, Belgium*; orcid.org/0000-0002-2989-3557

Complete contact information is available at: https://pubs.acs.org/10.1021/acs.jctc.2c00141

Notes

The authors declare no competing financial interest.

The research data supporting this publication can be accessed at https://doi.org/10.17630/fb9c92c6-675d-427e-b967-8fd94a0cb72c.

■ ACKNOWLEDGMENTS

The St Andrews team would like to thank the Leverhulme Trust (RPG-2016-047) for financial support. E.Z.C. is a Royal Society Leverhulme Trust Senior Research fellow (SRF\R1\201089). Computational resources have been provided by the Consortium des Équipements de Calcul Intensif (CÉCI), funded by the Fonds de la Recherche Scientifiques de Belgique (F.R.S.-FNRS) under Grant no. 2.5020.11, as well as the Tier-1 supercomputer of the Fédération Wallonie-Bruxelles, infrastructure funded by the Walloon Region under the grant agreement n1117545. G.R. acknowledges a grant from the "Fonds pour la formation à la Recherche dans l'Industrie et dans l'Agriculture" (F.R.I.A.) of the F.R.S.-F.N.R.S. Y.O. acknowledges funding by the Fonds de la Recherche Scientifique-FNRS under Grant n° F.4534.21 (MIS-IMAGINE). D.B. is a FNRS Research Director. J.C.S.G. acknowledges "Ministerio de Ciecia e Innovación" of Spain (PID2019-106114GB-I00).

■ REFERENCES

(1) Wong, M. Y.; Zysman-Colman, E. Purely Organic Thermally Activated Delayed Fluorescence Materials for Organic Light-Emitting Diodes. *Adv. Mater.* **2017**, *29*, 1605444.

(2) Liu, Y.; Li, C.; Ren, Z.; Yan, S.; Bryce, M. R. All-organic thermally activated delayed fluorescence materials for organic light-emitting diodes. *Nat. Rev. Mater.* **2018**, *3*, 18020.

(3) Yang, Z.; Mao, Z.; Xie, Z.; Zhang, Y.; Liu, S.; Zhao, J.; Xu, J.; Chi, Z.; Aldred, M. P. Recent advances in organic thermally activated delayed fluorescence materials. *Chem. Soc. Rev.* **2017**, *46*, 915–1016.

(4) Uoyama, H.; Goushi, K.; Shizu, K.; Nomura, H.; Adachi, C. Highly efficient organic light-emitting diodes from delayed fluorescence. *Nature* **2012**, *492*, 234–238.

(5) Tao, Y.; Yuan, K.; Chen, T.; Xu, P.; Li, H.; Chen, R.; Zheng, C.; Zhang, L.; Huang, W. Thermally Activated Delayed Fluorescence Materials Towards the Breakthrough of Organoelectronics. *Adv. Mater.* **2014**, *26*, 7931–7958.

(6) Hong, G.; Gan, X.; Leonhardt, C.; Zhang, Z.; Seibert, J.; Busch, J. M.; Bräse, S. A Brief History of OLEDs-Emitter Development and Industry Milestones. *Adv. Mater.* **2021**, *33*, 2005630.

(7) Etherington, M. K.; Gibson, J.; Higginbotham, H. F.; Penfold, T. J.; Monkman, A. P. Revealing the spin–vibronic coupling mechanism of thermally activated delayed fluorescence. *Nat. Commun.* **2016**, *7*, 13680.

(8) Moral, M.; Muccioli, L.; Son, W.-J.; Olivier, Y.; Sancho-García, J. C. Theoretical Rationalization of the Singlet–Triplet Gap in OLEDs Materials: Impact of Charge-Transfer Character. *J. Chem. Theory Comput.* **2015**, *11*, 168–177.

(9) Huang, S.; Zhang, Q.; Shiota, Y.; Nakagawa, T.; Kuwabara, K.; Yoshizawa, K.; Adachi, C. Computational Prediction for Singlet- and Triplet-Transition Energies of Charge-Transfer Compounds. *J. Chem. Theory Comput.* **2013**, *9*, 3872–3877.

(10) Jacquemin, D.; Planchat, A.; Adamo, C.; Mennucci, B. TD-DFT Assessment of Functionals for Optical 0-0 Transitions in Solvated Dyes. *J. Chem. Theory Comput.* **2012**, *8*, 2359–2372.

(11) Sun, H.; Zhong, C.; Brédas, J.-L. Reliable Prediction with Tuned Range-Separated Functionals of the Singlet–Triplet Gap in Organic Emitters for Thermally Activated Delayed Fluorescence. *J. Chem. Theory Comput.* **2015**, *11*, 3851–3858.

(12) Becke, A. D. A new mixing of Hartree–Fock and local density-functional theories. *J. Chem. Phys.* **1993**, *98*, 1372–1377.

(13) Adamo, C.; Barone, V. Toward reliable density functional methods without adjustable parameters: The PBE0 model. *J. Chem. Phys.* **1999**, *110*, 6158–6170.

(14) Cardeynaels, T.; Paredis, S.; Deckers, J.; Brebels, S.; Vanderzande, D.; Maes, W.; Champagne, B. Finding the optimal exchange–correlation functional to describe the excited state properties of push–pull organic dyes designed for thermally activated

delayed fluorescence. *Phys. Chem. Chem. Phys.* **2020**, *22*, 16387−16399.

(15) Zhao, Y.; Truhlar, D. G. The M06 suite of density functionals for main group thermochemistry, thermochemical kinetics, non-covalent interactions, excited states, and transition elements: two new functionals and systematic testing of four M06-class functionals and 12 other functionals. *Theor. Chem. Acc.* **2008**, *120*, 215−241.

(16) Vydrov, O. A.; Scuseria, G. E. Assessment of a long-range corrected hybrid functional. *J. Chem. Phys.* **2006**, *125*, 234109.

(17) Yanai, T.; Tew, D. P.; Handy, N. C. A new hybrid exchange−correlation functional using the Coulomb-attenuating method (CAM-B3LYP). *Chem. Phys. Lett.* **2004**, *393*, 51−57.

(18) Hatakeyama, T.; Shiren, K.; Nakajima, K.; Nomura, S.; Nakatsuka, S.; Kinoshita, K.; Ni, J.; Ono, Y.; Ikuta, T. Ultrapure Blue Thermally Activated Delayed Fluorescence Molecules: Efficient HOMO-LUMO Separation by the Multiple Resonance Effect. *Adv. Mater.* **2016**, *28*, 2777−2781.

(19) Madayanad Suresh, S.; Hall, D.; Beljonne, D.; Olivier, Y.; Zysman-Colman, E. Multiresonant Thermally Activated Delayed Fluorescence Emitters Based on Heteroatom-Doped Nanographenes: Recent Advances and Prospects for Organic Light-Emitting Diodes. *Adv. Funct. Mater.* **2020**, *30*, 1908677.

(20) Hall, D.; Suresh, S. M.; dos Santos, P. L.; Duda, E.; Bagnich, S.; Pershin, A.; Rajamalli, P.; Cordes, D. B.; Slawin, A. M. Z.; Beljonne, D.; Köhler, A.; Samuel, I. D. W.; Olivier, Y.; Zysman-Colman, E. Improving Processability and Efficiency of Resonant TADF Emitters: A Design Strategy. *Adv. Opt. Mater.* **2020**, *8*, 1901627.

(21) Ricci, G.; San-Fabián, E.; Olivier, Y.; Sancho-García, J. C. Singlet-Triplet Excited-State Inversion in Heptazine and Related Molecules: Assessment of TD-DFT and ab initio Methods. *ChemPhysChem* **2021**, *22*, 553−560.

(22) Sanz-Rodrigo, J.; Ricci, G.; Olivier, Y.; Sancho-García, J. C. Negative Singlet-Triplet Excitation Energy Gap in Triangle-Shaped Molecular Emitters for Efficient Triplet Harvesting. *J. Phys. Chem. A* **2021**, *125*, 513−522.

(23) Sanz-Rodrigo, J.; Olivier, Y.; Sancho-García, J.-C. Computational Studies of Molecular Materials for Unconventional Energy Conversion: The Challenge of Light Emission by Thermally Activated Delayed Fluorescence. *Molecules* **2020**, *25*, 1006.

(24) Pershin, A.; Hall, D.; Lemaur, V.; Sancho-Garcia, J.-C.; Muccioli, L.; Zysman-Colman, E.; Beljonne, D.; Olivier, Y. Highly emissive excitons with reduced exchange energy in thermally activated delayed fluorescent molecules. *Nat. Commun.* **2019**, *10*, 597.

(25) Hellweg, A.; Grün, S. A.; Hättig, C. Benchmarking the performance of spin-component scaled CC2 in ground and electronically excited states. *Phys. Chem. Chem. Phys.* **2008**, *10*, 4119−4127.

(26) Tajti, A.; Kozma, B.; Szalay, P. G. Improved Description of Charge-Transfer Potential Energy Surfaces via Spin-Component-Scaled CC2 and ADC(2) Methods. *J. Chem. Theory Comput.* **2021**, *17*, 439−449.

(27) Christiansen, O.; Koch, H.; Jørgensen, P. The second-order approximate coupled cluster singles and doubles model CC2. *Chem. Phys. Lett.* **1995**, *243*, 409−418.

(28) Knöller, J. A.; Meng, G.; Wang, X.; Hall, D.; Pershin, A.; Beljonne, D.; Olivier, Y.; Laschat, S.; Zysman-Colman, E.; Wang, S. Intramolecular Borylation via Sequential B-Mes Bond Cleavage for the Divergent Synthesis of B,N,B-Doped Benzo[4]helicenes. *Angew. Chem., Int. Ed.* **2020**, *59*, 3156−3160.

(29) Suresh, S. M.; Duda, E.; Hall, D.; Yao, Z.; Bagnich, S.; Slawin, A. M. Z.; Bässler, H.; Beljonne, D.; Buck, M.; Olivier, Y.; Köhler, A.; Zysman-Colman, E. A Deep Blue B,N-Doped Heptacene Emitter That Shows Both Thermally Activated Delayed Fluorescence and Delayed Fluorescence by Triplet-Triplet Annihilation. *J. Am. Chem. Soc.* **2020**, *142*, 6588−6599.

(30) Sun, D.; Suresh, S. M.; Hall, D.; Zhang, M.; Si, C.; Cordes, D. B.; Slawin, A. M. Z.; Olivier, Y.; Zhang, X.; Zysman-Colman, E. The design of an extended multiple resonance TADF emitter based on a polycyclic amine/carbonyl system. *Mater. Chem. Front.* **2020**, *4*, 2018−2022.

(31) Winter, N. O. C.; Hättig, C. Scaled opposite-spin CC2 for ground and excited states with fourth order scaling computational costs. *J. Chem. Phys.* **2011**, *134*, 184101.

(32) Tanaka, H.; Oda, S.; Ricci, G.; Gotoh, H.; Tabata, K.; Kawasumi, R.; Beljonne, D.; Olivier, Y.; Hatakeyama, T. Hypsochromic Shift of Multiple-Resonance-Induced Thermally Activated Delayed Fluorescence by Oxygen Atom Incorporation. *Angew. Chem., Int. Ed.* **2021**, *60*, 17910−17914.

(33) Petersson, G. A.; Al-Laham, M. A. A complete basis set model chemistry. II. Open-shell systems and the total energies of the first-row atoms. *J. Chem. Phys.* **1991**, *94*, 6081−6090.

(34) Dunning, T. H., Jr. Gaussian basis sets for use in correlated molecular calculations. I. The atoms boron through neon and hydrogen. *J. Chem. Phys.* **1989**, *90*, 1007−1023.

(35) Penfold, T. J. On Predicting the Excited-State Properties of Thermally Activated Delayed Fluorescence Emitters. *J. Phys. Chem. C* **2015**, *119*, 13535−13544.

(36) Frisch, M. J.; Trucks, G. W.; Schlegel, H. B.; Scuseria, G. E.; Robb, M. A.; Cheeseman, J. R.; Scalmani, G.; Barone, V.; Petersson, G. A.; Nakatsuji, H.; Li, X.; Caricato, M.; Marenich, A. V.; Bloino, J.; Janesko, B. G.; Gomperts, R.; Mennucci, B.; Hratchian, H. P.; Ortiz, J. V.; Izmaylov, A. F.; Sonnenberg, J. L.; Williams; Ding, F.; Lipparini, F.; Egidi, F.; Goings, J.; Peng, B.; Petrone, A.; Henderson, T.; Ranasinghe, D.; Zakrzewski, V. G.; Gao, J.; Rega, N.; Zheng, G.; Liang, W.; Hada, M.; Ehara, M.; Toyota, K.; Fukuda, R.; Hasegawa, J.; Ishida, M.; Nakajima, T.; Honda, Y.; Kitao, O.; Nakai, H.; Vreven, T.; Throssell, K.; Montgomery, J. A., Jr.; Peralta, J. E.; Ogliaro, F.; Bearpark, M. J.; Heyd, J. J.; Brothers, E. N.; Kudin, K. N.; Staroverov, V. N.; Keith, T. A.; Kobayashi, R.; Normand, J.; Raghavachari, K.; Rendell, A. P.; Burant, J. C.; Iyengar, S. S.; Tomasi, J.; Cossi, M.; Millam, J. M.; Klene, M.; Adamo, C.; Cammi, R.; Ochterski, J. W.; Martin, R. L.; Morokuma, K.; Farkas, O.; Foresman, J. B.; Fox, D. J. *Gaussian 16* Rev. A.01, Wallingford, CT, 2016.

(37) *TURBOMOLE V7.4*; TURBOMOLE GmbH, since 2007; avaliable from http://www.turbomole.com: a development of University of Karlsruhe and Forschungszentrum Karlsruhe GmbH, 2017.

(38) Etienne, T.; Assfeld, X.; Monari, A. Toward a Quantitative Assessment of Electronic Transitions' Charge-Transfer Character. *J. Chem. Theory Comput.* **2014**, *10*, 3896−3905.

(39) Etienne, T.; Assfeld, X.; Monari, A. New Insight into the Topology of Excited States through Detachment/Attachment Density Matrices-Based Centroids of Charge. *J. Chem. Theory Comput.* **2014**, *10*, 3906−3914.

(40) Dreuw, A.; Head-Gordon, M. Single-Reference ab Initio Methods for the Calculation of Excited States of Large Molecules. *Chem. Rev.* **2005**, *105*, 4009.

(41) Momma, K.; Izumi, F. VESTA 3 for three-dimensional visualization of crystal, volumetric and morphology data. *J. Appl. Crystallogr.* **2011**, *44*, 1272−1276.

(42) Yang, M.; Park, I. S.; Yasuda, T. Full-Color, Narrowband, and High-Efficiency Electroluminescence from Boron and Carbazole Embedded Polycyclic Heteroaromatics. *J. Am. Chem. Soc.* **2020**, *142*, 19468−19472.

(43) Qi, Y.; Ning, W.; Zou, Y.; Cao, X.; Gong, S.; Yang, C. Peripheral Decoration of Multi-Resonance Molecules as a Versatile Approach for Simultaneous Long-Wavelength and Narrowband Emission. *Adv. Funct. Mater.* **2021**, *31*, 2102017.

(44) Liu, Y.; Xiao, X.; Ran, Y.; Bin, Z.; You, J. Molecular design of thermally activated delayed fluorescent emitters for narrowband orange−red OLEDs boosted by a cyano-functionalization strategy. *Chem. Sci.* **2021**, *12*, 9408−9412.

(45) Cai, X.; Xu, Y.; Wang, Q.; Li, C.; Wang, Y. Constructing Narrowband Thermally Activated Delayed Fluorescence Materials with Emission Maxima Beyond 560 nm Based on Frontier Molecular Orbital Engineering. *ChemRxiv* **2021**, DOI: 10.26434/chem-rxiv.14371073.v1.

(46) Lu, T.; Chen, F. Multiwfn: a multifunctional wavefunction analyzer. *J. Comput. Chem.* **2012**, *33*, 580−592.
(47) Olivier, Y.; Sancho-Garcia, J.-C.; Muccioli, L.; D'Avino, G.; Beljonne, D. Computational Design of Thermally Activated Delayed Fluorescence Materials: The Challenges Ahead. *J. Phys. Chem. Lett.* **2018**, *9*, 6149−6163.
(48) Savarese, M.; Guido, C. A.; Brémond, E.; Ciofini, I.; Adamo, C. Metrics for Molecular Electronic Excitations: A Comparison between Orbital- and Density-Based Descriptors. *J. Phys. Chem. A* **2017**, *121*, 7543−7549.
(49) Stavrou, K.; Danos, A.; Hama, T.; Hatakeyama, T.; Monkman, A. Hot Vibrational States in a High-Performance Multiple Resonance Emitter and the Effect of Excimer Quenching on Organic Light-Emitting Diodes. *ACS Appl. Mater. Interfaces* **2021**, *13*, 8643−8655.
(50) Hättig, C.; Köhn, A.; Hald, K. First-order properties for triplet excited states in the approximated coupled cluster model CC2 using an explicitly spin coupled basis. *J. Chem. Phys.* **2002**, *116*, 5401−5410.
(51) Cui, L.-S.; Gillett, A. J.; Zhang, S.-F.; Ye, H.; Liu, Y.; Chen, X.-K.; Lin, Z.-S.; Evans, E. W.; Myers, W. K.; Ronson, T. K.; Nakanotani, H.; Reineke, S.; Bredas, J.-L.; Adachi, C.; Friend, R. H. Fast spin-flip enables efficient and stable organic electroluminescence from charge-transfer states. *Nat. Photonics* **2020**, *14*, 636−642.
(52) Zysman-Colman, E. Molecular designs offer fast exciton conversion. *Nat. Photonics* **2020**, *14*, 593−594.
(53) Noda, H.; Chen, X.-K.; Nakanotani, H.; Hosokai, T.; Miyajima, M.; Notsuka, N.; Kashima, Y.; Brédas, J.-L.; Adachi, C. Critical role of intermediate electronic states for spin-flip processes in charge-transfer-type organic molecules with multiple donors and acceptors. *Nat. Mater.* **2019**, *18*, 1084−1090.
(54) Kim, I.; Cho, K. H.; Jeon, S. O.; Son, W.-J.; Kim, D.; Rhee, Y. M.; Jang, I.; Choi, H.; Kim, D. S. Three States Involving Vibronic Resonance is a Key to Enhancing Reverse Intersystem Crossing Dynamics of an Organoboron-Based Ultrapure Blue Emitter. *JACS Au* **2021**, *1*, 987−997.
(55) Min, H.; Park, I. S.; Yasuda, T. cis-Quinacridone-Based Delayed Fluorescence Emitters: Seemingly Old but Renewed Functional Luminogens. *Angew. Chem., Int. Ed.* **2021**, *60*, 7643−7648.
(56) Northey, T.; Penfold, T. J. The intersystem crossing mechanism of an ultrapure blue organoboron emitter. *Org. Electron.* **2018**, *59*, 45−48.
(57) Kim, H. J.; Godumala, M.; Kim, S. K.; Yoon, J.; Kim, C. Y.; Park, H.; Kwon, J. H.; Cho, M. J.; Choi, D. H. Color-Tunable Boron-Based Emitters Exhibiting Aggregation-Induced Emission and Thermally Activated Delayed Fluorescence for Efficient Solution-Processable Nondoped Deep-Blue to Sky-Blue OLEDs. *Adv. Opt. Mater.* **2020**, *8*, 1902175.
(58) Meng, G.; Chen, X.; Wang, X.; Wang, N.; Peng, T.; Wang, S. Isomeric Bright Sky-Blue TADF Emitters Based on Bisacridine Decorated DBNA: Impact of Donor Locations on Luminescent and Electroluminescent Properties. *Adv. Opt. Mater.* **2019**, *7*, 1900130.
(59) Yuan, Y.; Tang, X.; Du, X. Y.; Hu, Y.; Yu, Y. J.; Jiang, Z. Q.; Liao, L. S.; Lee, S. T. The Design of Fused Amine/Carbonyl System for Efficient Thermally Activated Delayed Fluorescence: Novel Multiple Resonance Core and Electron Acceptor. *Adv. Opt. Mater.* **2019**, *7*, 1801536.
(60) Hirai, H.; Nakajima, K.; Nakatsuka, S.; Shiren, K.; Ni, J.; Nomura, S.; Ikuta, T.; Hatakeyama, T. One-Step Borylation of 1,3-Diaryloxybenzenes Towards Efficient Materials for Organic Light-Emitting Diodes. *Angew. Chem., Int. Ed.* **2015**, *54*, 13581−13585.
(61) Karthik, D.; Ahn, D. H.; Ryu, J. H.; Lee, H.; Maeng, J. H.; Lee, J. Y.; Kwon, J. H. Highly efficient blue thermally activated delayed fluorescence organic light emitting diodes based on tercarbazole donor and boron acceptor dyads. *J. Mater. Chem. C* **2020**, *8*, 2272−2279.
(62) Song, D.; Yu, Y.; Yue, L.; Zhong, D.; Zhang, Y.; Yang, X.; Sun, Y.; Zhou, G.; Wu, Z. Asymmetric thermally activated delayed fluorescence (TADF) emitters with 5,9-dioxa-13b-boranaphtho-[3,2,1-de]anthracene (OBA) as the acceptor and highly efficient blue-emitting OLEDs. *J. Mater. Chem. C* **2019**, *7*, 11953−11963.
(63) Kim, J. U.; Park, I. S.; Chan, C.-Y.; Tanaka, M.; Tsuchiya, Y.; Nakanotani, H.; Adachi, C. Nanosecond-time-scale delayed fluorescence molecule for deep-blue OLEDs with small efficiency rolloff. *Nat. Commun.* **2020**, *11*, 1765.
(64) Ahn, D. H.; Kim, S. W.; Lee, H.; Ko, I. J.; Karthik, D.; Lee, J. Y.; Kwon, J. H. Highly efficient blue thermally activated delayed fluorescence emitters based on symmetrical and rigid oxygen-bridged boron acceptors. *Nat. Photonics* **2019**, *13*, 540−546.
(65) Olivier, Y.; Yurash, B.; Muccioli, L.; D'Avino, G.; Mikhnenko, O.; Sancho-García, J. C.; Adachi, C.; Nguyen, T. Q.; Beljonne, D. Nature of the singlet and triplet excitations mediating thermally activated delayed fluorescence. *Phys. Rev. Mater.* **2017**, *1*, 075602.
(66) Wu, X.; Su, B.-K.; Chen, D.-G.; Liu, D.; Wu, C.-C.; Huang, Z.-X.; Lin, T.-C.; Wu, C.-H.; Zhu, M.; Li, E. Y.; Hung, W.-Y.; Zhu, W.; Chou, P.-T. The role of host−guest interactions in organic emitters employing MR-TADF. *Nat. Photonics* **2021**, *15*, 780−786.
(67) Phan Huu, D. K. A.; Dhali, R.; Pieroni, C.; Di Maiolo, F.; Sissa, C.; Terenziani, F.; Painelli, A. Antiadiabatic View of Fast Environmental Effects on Optical Spectra. *Phys. Rev. Lett.* **2020**, *124*, 107401.
(68) Gillett, A. J.; Pershin, A.; Pandya, R.; Feldmann, S.; Sneyd, A. J.; Alvertis, A. M.; Evans, E. W.; Thomas, T. H.; Cui, L.-S.; Drummond, B. H.; Scholes, G. D.; Olivier, Y.; Rao, A.; Friend, R. H.; Beljonne, D. Dielectric control of reverse intersystem crossing in thermally-activated delayed fluorescence emitters. **2021**, arXiv:2109.05945.

https://doi.org/10.1021/acs.jctc.2c00141
J. Chem. Theory Comput. 2022, 18, 4903−4918